

An-Najah National University
Faculty of Graduate Studies

**Zeolite/Cellulose Acetate (ZCA) in Blend
Fiber for Removal of Erythromycin from
Aqueous Solution Experimental and
Theoretical Study**

By
Israa Faisal Ahmed Erman

Supervisors
Prof. Shehdeh Jodeh
Prof. Othman Hamed

**This Thesis is Submitted in Partial Fulfillment of the Requirements for
the Degree of Master of Chemistry, Faculty of Graduate Studies, An-
Najah National University, Nablus, Palestine.**

2021

**Zeolite /Cellulose Acetate (ZCA) in Blend Fiber for
Removal of Erythromycin from Aqueous Solution
Experimental and Theoretical Study**

By

Israa Faisal Ahmed Erman

This Thesis was defended successfully on 24/8/2021 and approved by:

Defense Committee Members

Signature

– **Prof. Shehdeh Jodeh / Supervisor**

.....
Shehdeh Jodeh

– **Prof. Othman Hamed/ Co- Supervisor**

.....
Othman Hamed

– **Dr. Subhi Samhan / External Examiner**

.....
Subhi Samhan

– **Dr. Dirar El Smadi/Internal Examiner**

.....
Dirar El Smadi

Dedication

Praise be to God Almighty, Lord of the worlds before and after, this message is dedicated to all members of my family for their unlimited love and encouragement, especially my wonderful mother who created me from nothingness; She was literally ready to do anything for us in the most difficult circumstances, and to my wonderful father and my first supporter, to my children Nour and Sultan, and to their dear father, and I also dedicate this work to my creative and distinguished doctors and professors who had a great role in my personal development and my thinking in many from the aspects, whether in the cognitive or moral side. And to my colleagues Oraib, Walaa Odeh, and my great friends who always stand by me firmly at critical moments, it's hard to list all the names here but you are always on my mind. Words will never express how grateful I am to all of you so I hope my actions will one day express it. Finally, we will never finish the work, and these are just stops in our lives while the sky will be the limit. Praise be to God who wrote this success for us.

Acknowledgments

When you arrive, do not forget who paved the way for you. I would like to confess my sincere appreciation to my supervisors Prof. ShehdehJodeh and prof. Othman Hamed for their exclusive and creative advice that made a great experience on a personal level until this work come to existence. Many thanks also to Dr. Ghadir Hanbali and Younes Massad for their ongoing support. I also would take this opportunity to grant my thanks to all the technicians and faculty members in department of chemistry at An-Najah national university, especially Mr. Nafiz Dweikat for help. Dr.Nawaf Al-Mahariq and others, they didn't skimp on me even by the smallest things,it really was an amazing experience to deal with such inspired people.

الإقرار

انا الموقع ادناه مقدم الرسالة التي تحمل عنوان:

Zeolite/Cellulose Acetate (ZCA) in Blend Fiber for Removal of Erythromycin from Aqueous Solution Experimental and Theoretical Study

أقر بان ما اشتملت عليه هذه الرسالة انما هي نتاج جهدي الخاص، باستثناء ما تم الاشارة اليه حيثما ورد، وان هذه الرسالة ككل، او اي جزء منها لم يقدم لنيل اي درجة او لقب علمي او بحثي لدى اي مؤسسة تعليمية او بحثية اخرى.

Declaration

The work provided in this thesis, unless otherwise referenced, is the researcher's own work, and has not been submitted elsewhere for any other degree or qualifications.

Student's Name:

اسم الطالبة: إسرائ فيصل احمد عرمان

Signature:

التوقيع: إسرائ فيصل احمد عرمان

Date:

التاريخ : 2021/8/24

Table of Content

Dedication	III
Acknowledgments	IV
Declaration	V
Table of Content.....	VI
List of Figures	X
List of Tables.....	IX
List of Abbreviations.....	XII
Abstract	XIV
Chapter One: Introduction	1
1.2 Research Objective	3
1.3 Research questions.....	4
Chapter Two: Literature review	5
2.1 Water problem.....	5
2.1.1Pharmaceutical wastewater.....	6
2.2 Erythromycin	7
2.3 Waste Water Treatment Plant (WWTPs).....	9
2.3.1 Methods of Advanced treatment of pharmaceutical wastewater...	9
2.3.2 Cellulose Acetate (CA).....	11
2.3.3 Zeolites.....	12
2.3.4 Zeolitic Imidazolate framework (ZIF-L).....	14
2.3.5 CA/ZA Membrane morphology	15
2.4 Adsorption process.....	16
2.4.1 Langmuir Adsorption Isotherm	17
2.4.2 Freundlich Adsorption Isotherm.....	19
2.5 Adsorption Kinetic Models.....	20
2.5.1 Pseudo 1 st Order Kinetics	20

VII

2.5.2 Pseudo 2 nd Order Kinetics.....	21
2.6 Adsorption Thermodynamics.....	22
2.7 Analytical Techniques	23
Chapter Three: Experimental Part.....	24
3.1 Instrumentation	24
3.2 Chemicals and materials	24
3.3 Methodology	25
3.3.1 Synthesis of cellulose acetate	25
3.3.2 Preparation of ZCAB fiber	26
3.3.3 Characterization of ZCAB fiber	26
3.4 Calibration Curves	27
3.5 Batch Adsorption Experiments	29
3.5.1 Effect of contact time.....	30
3.5.2 Effect of PH	30
3.5.3 Effect of temperature	31
3.5.4 Effect of adsorbent dose	32
3.6 Computational and Theoretical Study	33
Chapter Four: Results and Discussion	35
4.1 Adsorbent characterization results (BET).....	35
4.1.2 Characterization of ZCA fiber using SEM	35
4.1.3 X-ray diffraction analysis	37
4.1.4 FT-IR analysis.....	38
4.1.5. Thermo gravimetric analysis (TGA).	39
4.1.6. Differential scanning calorimetry (DSC).	41
4.2 Results of Adsorption	42
4.2.1 Effect of contact time.....	43
4.2.2 Effect of temperature	45
4.2.3 Effect of Adsorbate Initial Concentration	46

VIII

4.3 Equilibrium Isotherm Models	49
4.4 Adsorption kinetic models	51
4.5 Adsorption thermodynamic	54
4.6 Quantum Chemical Studies.....	55
4.7 Desorption study	60
4.8 Conclusion	61
4.8 Recommendations	62
References	64
المخلص	ب

List of Tables

Table 1: Typical characteristics of pharmaceutical effluents.....	6
Table.2: Examples of Antibiotic Concentrations in Wastewater and River Water [33].....	8
Table 3: Previous studies on ERY removal from water.....	48
Table 4: The parameters of Langmuir and Freundlich isotherms for the adsorption of ERY on ZCAB.....	51
Table 5: the parameters of pseudo-1st-order, pseudo-2nd-order for the adsorption of ERY onto ZCAB.....	53
Table 6: the thermodynamic parameters for the adsorption of ERY on ZCAB.....	54
Table 7: The calculated physical and quantum chemical quantities of ERY at HF/6-311G** level.....	57
Table 8: NBO Results for ERY at HF/6-311G** level.....	60

List of Figures

Figure 1. Structure Of Erythromycin	8
Figure 2: Advantages and disadvantages of some used wastewater treatment technique.....	10
Figure3: Structure of cellulose triacetate, n is typically 400–1000	12
Figure 4: SEM image and crystal structure of ZIF-L	14
Figure 5: SEM images of cross section CA membrane(a), CA/ZA membrane(b), distribution of silica from zeolite (c), alumina from zeolite (d).....	16
Figure 6: different adsorption isotherm models	17
Figure 7: preparation of cellulose acetate	25
Figure 8: calibration curve for ERY standard solution using UV instrument.....	28
Figure9: SEM images of (a) ZCA fiber b) Zeolite c) cellulose acetate (CA).....	36
Figure10: Comparison of X-ray Diffractograms of: (a) Zeolite, (b) CA and (c)ZCA.....	37
Figure11: FT-IR for ZCA a) before adsorption and b) after adsorption process of ERY.....	39
Figure12: Thermogravimetric analysis (TGA) for (a) Zeolite\CA(ZCA), (b) CA and (c) zeolite.....	41
Figure13: Differential scanning calorimetry (DSC) for cellulose acetate film (CA) and cellulose acetate/Zeolite (ZCA).....	42
Figure 14: effect of contact time on the removal of ERY using ZCAB.....	44
Figure15: effect of temperature on the removal of ERY using ZCAB.....	45
Figure16: Effect of initial concentration on the adsorption of ERY on to ZCAB.....	47

Figure17: Adsorption isotherm models: a) Freundlich, b) Langmuir models for ERY using three different adsorbents.....50

Figure 18: Kinetic models of for the adsorption of ERY by the three adsorbents at different time periods a) pseudo first order, b) pseudo second order, c) intraparticle diffusion.....53

Figure 19: The optimized structures of ERY at HF/6-311G** level (left site with Hs and right side without Hs).....57

Figure 20: HOMO and LUMO (isoval:0.02), and MEP (isoval:0.0004) plots of ERY at HF/6-311G** level.....58

Figure21: Three cycles for each adsorbent showing excellent reuse.....61

List of Abbreviations

Symbol	Abbreviation
G	gram.
Mg	milligram.
L/g	Liter per gram.
J	Joule.
K	Kelvin.
J/K	Joule per kelvin.
KJ/mol	Kilojoule per mole.
AC	Activated carbon.
A	Arrhenius factor.
C _e	Adsorbed concentration at equilibrium (mg/L).
C _o	The initial concentration of the adsorbed (mg/L).
E _a	Arrhenius Activation Energy (KJ/mole).
EPA	Environmental Protection Agency.
K _L	Langmuir Isotherm Constant (L/mg).
K _F	Freundlich Constant (mg/g).
K ₁	The rate constant of pseudo 1st-order (min ⁻¹).
K ₂	The rate constant of pseudo 2nd-order (mg/g.min ⁻¹).
K _{id}	The intra-particle diffusion rate constant (mg/g.min ^{-1/2}).
K _d	The thermodynamic equilibrium constant (L/g).
q _e	The amount of adsorbed per unit mass of adsorbent (mg/g).
q _L	The maximum monolayer coverage capacity (mg/g).
q _t	The mass of adsorbed per unit mass of adsorbent at any time (mg/g)
R	The universal gas constant (8.314 J/mol.K).
K _{oc}	Soil Sorption Coefficient
LD ₅₀	Lethal Dose that causes death at 50% of the treated animal.
ΔS°	Standard entropy change (J/K).
T	The absolute temperature (K).
T	Time (min).
TEM	Transmission electron microscopy.
UV-Vis	Ultraviolet Visible spectroscopy.
V	The volume of the solution (L).
WWTP	Waste water Treatment Plant.
W	Mass of adsorbent (g).
OPPs	Organophosphorus Pesticides.

XIII

ZCAB	Zeolite/cellulose Acetate in Blend fiber.
ERY	Erythromycin.
CA	Cellulose Acetate.
2-PEA	2-PhenylEthylAmine.
DS	Degree of Substitution.
US-EPA	United States Environmental Protection Agency.
Z	Zeolite.
CAS	Chemical Abstract Number.
QCP _s	Quantum Chemical Parameters
ERY	Erythromycin
CA/ZA	Cellulose Acetate /Zeolite .A
EPA	Environmental Protection Agency
CEC _s	Contaminants of Emerging Concern
r.p.m	rotation per minute
ppt	part per million
ppb	Part per billion
TLV	Threshold Limit Value
WHO	World Health Organization
NOM	Natural Organic Matter
SPE	Solid Phase Extraction
BET	Brunauer Emmett Teller

**Zeolite/Cellulose Acetate (ZCA) in Blend Fiber for Removal of
Erythromycin from Aqueous Solution Experimental
and Theoretical Study**

By

Israa Faisal Ahmed Erman

Supervisors

Prof. Shehdeh Jodeh

Prof. Othman Hamed

Abstract

The highly use of pharmaceutical products in various areas has led to the worldwide pollution in the environment. However, effective purification of water contaminated by erythromycin antibiotics remains a great challenge. The more since, wastewater treatment plants are not capable of removing effectively the antibiotics. The aim of this study is to improve the performance of zeolite-A as an adsorbent material using cellulose acetate (CA) addition as a support membrane, for erythromycin antibiotics adsorption. The membrane is called as Cellulose Acetate/Zeolite-A (CA/ZA) membrane. The number of interchangeable sites in the adsorbent structures and the ratio of erythromycin to the three adsorbents were identified as the main reasons for the reduction in adsorption as the initial ERY concentrations increased. Additionally, to pseudo-first-order modelling for all adsorbents, the pseudo second-order modeling showed better fitting for the adsorption. However, the findings obtained in pseudo-first-order model were still enough for explaining the sorption kinetics of ERY, showing that the surface displayed all chemi-sorption and physi-sorption adsorption processes by both adsorbents. Also, the Langmuir and Freundlich isotherm

model were discussed to find that this adsorption isotherm was fitted better by Langmuir. The three adsorbents showed negative values of ΔH and these values were -6200, -8500 and -9600 KJ/mol for zeolite, CA and ZCA respectively and this shows that the adsorption is exothermic. In addition, the chemical attitude and possible donor-acceptor interactions of the ERY were assessed by the quantum chemical parameters (QCPs) and NBO analysis performed, at the HF/6-311G** calculations. The desorption analysis shows no substantial loss of adsorption site after three runs, indicating the higher stability and resilience of the three adsorbents, indicating a strong repeatability of their possible use in adsorption processes without contaminating the environment.

Chapter One

Introduction

The capacity of a society to supply fresh water for hygiene and consumption to the population is perhaps one of the most significant factors for the sustainable development of developed countries and the extension of urban areas. However, with a growth in population and urbanization, the leakage of toxic material into the atmosphere and surface water is also increasing. Sources of surface and groundwater pollution are wide, including agricultural, manufacturing, oil pollution, sewage and wastewater [1, 2].

Environmental samples such as surface water, groundwater, seawater, soil and drinking water, pharmaceuticals were found [3, 4], So they're referred to as emerging pollutants. The estimated global consumption of pharmaceuticals such as antibiotics is 100,000 to 200,000 tons per year[5]. Based on the chemical properties of the drug, about 5- 90% of the absorbed antibiotic doses are excreted by urine or stool as a metabolite or parent compound [6]. These drugs end up in drainage systems and eventually reach the ecosystem by sewage leakage, discharge of wastewater treatment plant (WWTP) effluents into marine systems, or disposal of unwanted or unfinished medications [7]. The use of sludge and animal waste as fertilizer in agriculture can also contribute to degradation of agricultural soils which can lead to the incorporation of antibiotics into marine environments by leaching into groundwater [8].

In recent years, the Environmental Protection Agency (EPA) has gotten proactive in advising the society about Contaminants of Emerging Concern (CECs). CECs are a class of pollutants that are typically detected at trace levels in surface and groundwater (i.e., ppb, ppt). Instances of CECs are pesticides, chemicals, anti-infection agents, over-the-counter meds, rural side-effects, mechanical synthetics, oil based synthetic compounds, and others [9]. In particular, some of these methods do not have actual removal techniques, and the by-products that are generated, such as organochlorine organisms, can be more harmful than the original compounds [10].

To deal with this wastewater problem, lots of conventional and advanced technologies have been developed [11]. The conventional water treatments such as oxidation [12], electro precipitation, membrane separation, coagulation-flocculation, evaporation, floatation, and ion [13] exchange have been largely used but these are inadequate techniques for water treatments [14].

Among various pharmaceuticals [15], antibiotics are widely used to prevent and treat diseases and infections, as well as to promote the growth of human and animals. These antibiotics are released into the water environment in their metabolized and non-metabolized forms. After years of abuse, antibiotics, which pose series of threats to the ecosystem and human health as well as induce proliferation of bacterial drug resistance, are extensively found in aquatic environment. Therefore, the removal of antibiotics from the environment has become a mandatory issue [16, 17]. As a result, there is an

urgent need to develop a convenient and reliable approach to tackle environmental problems related to antibiotics residue. Different methods for water treatment and removal of new emerging pollutants were developed and reported. These methods include filtration, screening, oxidation, precipitation, coagulation, centrifugation, flotation, crystallization, sedimentation, distillation, evaporation, reverse osmosis, electro chemical, ion exchange, adsorption etc. Most of these methods suffer from disadvantages such as low treatment efficiency, inconvenience of foster microbe, expensive analysis settings, or labor-intensive sample preparation, which limit their application and need further improvement [16]. Among these methods, adsorption phenomenon is considered as one of the appropriate water treatment methodology because of its ease of operation, low cost and the accessibility with a wide range of adsorbents. Examples on the adsorbents are activated carbon, later on was replaced by some cost-effective adsorbents [18, 19]. Concentrations of antibiotics and synthetic antimicrobial drugs from mg/L up to a few mg/L have been observed in wastewater and surface waters. However, certain point sources such as waste streams and effluents generated by hospitals, pharmaceutical production facilities, concentrated animal feeding operations, and aquaculture may have much higher antimicrobial concentrations, on the order of a few mg/L.

1.2 Research Objective

1. To prepare Zeolite /Cellulose Acetate (ZCA) in blend fiber, then use it to remove of Erythromycin residue.

2. To optimizing different parameters that affects the adsorption process.
3. To study the kinetic, isotherm, and thermodynamic data for the adsorption of erythromycin onto adsorbent in different cases.

1.3 Research questions

1. Is Zeolite/cellulose acetate (ZCA) in blend fiber for adsorption of erythromycin residue from pharmaceutical wastewater are ideal for new emergent pollutants as these contaminates are present at very low concentrations?
2. Could this method be appropriate, reliable and selective remove of erythromycin from wastewater?
3. What are the optimum conditions for the removal of erythromycin residue using Zeolite/cellulose acetate (ZCA) in blend fiber?

Chapter Two

Literature review

2.1 Water problem

water is the secret of life, what is that novel molecules nothing can exist without it and it needs no one to exist, water just go throw a cycle starts from evaporating water bodies to the stage of condenses as a clouds in the sky to rain it again, there is some impurities at low quantity enters to the water in the normal case from a living or natural sources and there is no problem, the main one arise from uncontrolled amount that escape into the water at either stages of its cycle[20].

Groundwater, as one of the major fresh water resources, is a part of the water cycle, and is a decreasing water resource, it makes up approximately 30% of the total worlds freshwater. During the recharge process for groundwater, which is refers to the downward movement of water from the unsaturated zone to the saturated one, rain water take a lots of impurities and pollutant throw this traveling [20], The quality of groundwater in most areas is very good, it usually needs less treatment than surface water in order to make it safe for drinking [21], this is because of flowing of groundwater through the soil and rocks play an important role in the removal of different type of pollutant, here a major source of pollution which occur by ether organics or inorganics or even biological compounds, so these chemical pollutant escape into the surface water at more than allowable specific amount depending on the type and toxicity of that pollutant, this amount called Threshold Limit

Value (TLV), which shows the average concentration to which any person with good health may be exposed for seven or eight hours per week for lifetime without showing an adverse health effect[22].

In the last decades, this pollutant spread over as commercial products to meet human needs and a high demands on other essential requirement from agricultural, pharmaceutical and personal care product, because of water is considered a universal solvent; it can easily dissolve many types of materials, according to the World Health Organization (WHO) guidelines for drinking water at third edition 2008 in Geneva about six hundred chemicals have been listed with threshold limit values ranging from very low concentrations such as 0.001 ppm for mercury to a high value like 1000 ppm for others[23], so in general the pollution of groundwater become larger in the presence of industrial activity.

2.1.1Pharmaceutical wastewater.

Various constituents of pharmaceutical wastewater is described in (Table1)[24].

Table 1: Typical characteristics of pharmaceutical effluents

Parameter	Standard effluent Values
Biological Oxygen demand, BOD	900 – 400 ppm
Chemical Oxygen demand, COD	2000 – 6000 ppm
Acidity, Ph	1.5 – 6.0
Oil and Grease	35 – 2000 ppm
Total dissolved solid, TDS	1350 – 7250 ppm
Total suspended solid, TSS	500 – 2000 ppm
Total Kjeldahl nitrogen, TKN	800 – 1000 ppm

Further complication for treatment approach is by making general ways, it is turns to be difficult in this case because of poor empirical relations of pharmaceutical compounds, wastewater characteristics and the operational parameters of flow and Hydraulic Retention Time (HRT) [24]. The properties of used pharmaceutical wastewater in varied between the common kinds, so there is so much properties to be studied and characterized, among the so much criteria is sulfate amounts and toxicity. Other countries have others properties to fit with take Chinese patent characterization of wastewater [25].

2.2 Erythromycin

Erythromycin (ERY) is an antibiotic that is commonly used to treat a number of bacterial infections. After therapy remains constant, antibiotics move through the human body and eventually reach the inland areas and the effluents, there is also a road of environmental contamination in the poultry and livestock breeding industry. ERY molecules are resistant to the environment due to the composition of their aromatic ring, which makes it difficult to degrade [26]. The existence of ERY in water and wastewater has been confirmed to be above the normal level in different studies [27, 28]. Subsequently, the removal of ERY residues from wastewater is important [29].

The main component of erythromycin is erythromycin A (EA) which has a molecular formula of $C_{37}H_{67}NO_{13}$, molecular weight is 733.93. Molecular structure for ERY A is shown in Fig.1 [30].

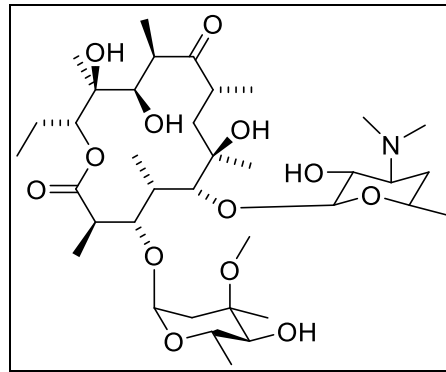


Figure 1. Structure Of Erythromycin A[30]

Macrolides consist of macro cyclic lactones structures to prevent bacterial growth by binding to the 23S ribosomal RNA and inhibiting protein synthesis. Mechanisms of resistance to macrolides include efflux of the antimicrobials and alteration of the target site (through methylation of a specific nucleotide in the 23S ribosomal RNA) so that it can no longer bind the antimicrobials [31, 32]. Examples of antibiotic concentrations in wastewater and river water are presented in Table 2 [33].

Table.2: Examples of Antibiotic Concentrations in Wastewater and River Water [33].

	Antibiotic	Type	Concentration ($\mu\text{g/L}$)		
			Median	Min	Max
Raw urban wastewater influents	Erythromycin-H ₂ O	Macrolide	0.34	0.07	1.2
	Erythromycin-H ₂ O	Macrolide	0.63	0.47	0.81
	Azithromycin	Macrolide	0.7	0.09	0.38
Hospital effluents	Erythromycin-H ₂ O	Macrolide	0.94		6.11
	Ciprofloxacin	Fluoroquinolone		3	87
Drug manufacture effluents	Erythromycin-H ₂ O	Macrolide	0.11		7.8
Urban wastewater treatment plant treated effluents	Erythromycin-H ₂ O	Macrolide	0.27	0.09	0.3
River water	Azithromycin	Macrolide	0.037	0.02 2	0.169

2.3 Waste Water Treatment Plant (WWTPs).

Since pollution of water did not occur by just one type of pollutant, water treatment process must deal with all of these materials in water taking in account the differences in a nature, size, amount that is done by going through several steps starting with a physical separations at macro scale for larger molecule and heavy material to be filtered and precipitated which is sometimes considered an easy to do, then finished at a micro scale to treat with a very low pollutant concentration, and other biological matter presents in the water, like this pesticide materials amount to get it in the accepted range for human uses [34]

2.3.1 Methods of Advanced treatment of pharmaceutical wastewater

A lots of methods were performed for pesticides treatment including Ozone as chemical oxidation [35], membrane separation, biological degradation, ion exchange, photo degradation ,chemical precipitation, and adsorption [35-37]. Among this, adsorption is the best method since its consider relatively more effective with contrast to other classical methods because of its low operation cost, reusability of the adsorbent, selectivity improvement for some specific adsorbate and also its ability to treat target adsorbate in higher concentrated form [38, 39], the following figure shows the main advantages and disadvantages for several main techniques of wastewater treatment.

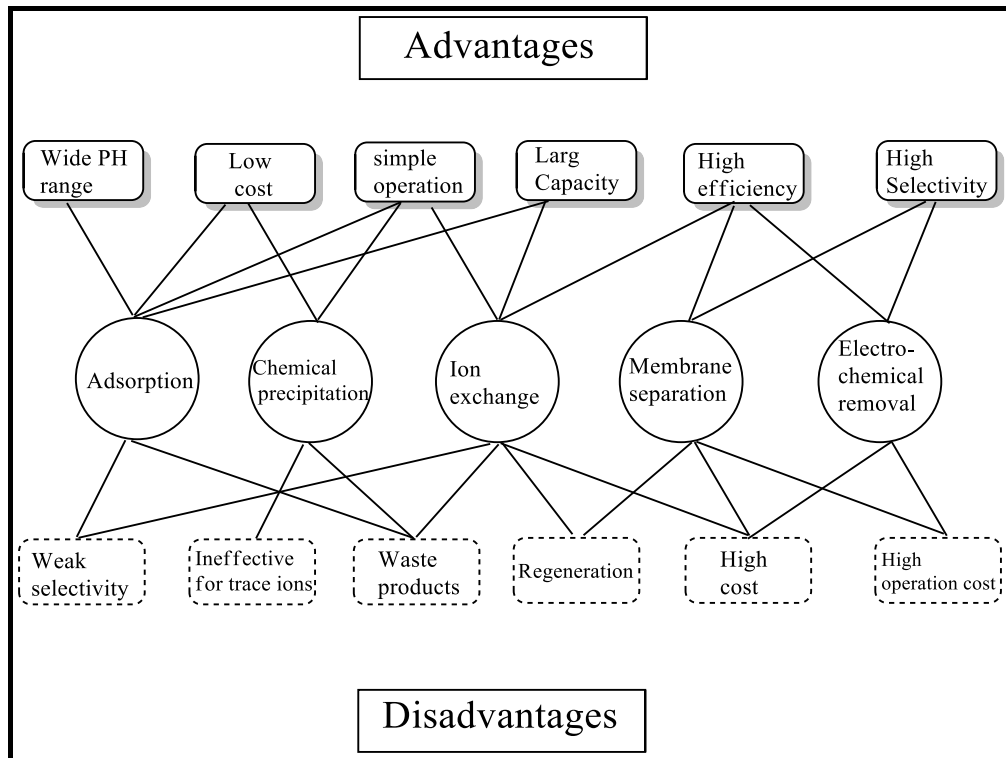


Figure 2: Advantages and disadvantages of some used wastewater treatment technique.

Several studies have been successfully performed to study different types of cost effective and locally available materials as adsorbent for the removal of several pesticides [40-44].

Despite that, the using of these types of adsorbent associated with some disadvantages including incompatible in operating columns due to non-spherical nature such that resulting in exhausted for industrial columns, adsorption of pesticides at moderately low amount, high cost for the regeneration process and small scale production of carbon materials. furthermore, other methods such as reverse osmosis, Nano filtration and advanced oxidation processes are not desirable because it form undesirable oxidized by products and exposed also to membrane fouling [45]. Despite,

prepared resins are moderately more expensive but it may be designed to exhibit more selectivity and adsorption capacity for specific target pollutants than Activated Carbon. Strong potential for the removal of Natural Organic Matter(NOM) and pesticides have been showed by Anion exchange resins [46, 47].

Separation techniques can classified into two main category depending on the way that adsorption occur that results in batch and continuous adsorption in which analyte are adsorbed on to materials that insoluble in water as it known also as Solid Phase Extraction (SPE) [48, 49]. For the materials to be beneficial in it should be synthesized easily, and have a quantitative and reproducible collection to be eluted with minimum efforts exerted in experimental steps.

2.3.2 Cellulose Acetate (CA)

Cellulose acetate refers to any acetate ester of cellulose, usually cellulose diacetate. It was first prepared in 1865. (CA) which are obtained by reaction of cellulose with acetic anhydride and acetic acid in the presence of sulfuric acid. The most common form of cellulose acetate fiber has an acetate group on approximately 2–2.5 of every three hydroxyls. This cellulose diacetate is known as secondary acetate, or simply as “acetate”. The solubility of cellulose acetate depends among other things on the Degree of Substitution (DS), CA with DS of 2 – 2.5 is soluble e. g. in acetone, dioxane and methyl acetate; higher acetylated types are soluble in dichloromethane. Acetic acid is in generally a

good solvent for cellulose acetates with DS greater than 0.8[50].

Cellulose acetate is prepared by acetylating cellulose, the most abundant natural polymer. Cellulose is readily biodegraded by organisms that utilize cellulose enzymes, but due to the additional acetyl groups cellulose acetate requires the presence of esterase for the first step in biodegradation. Once partial deacetylation has been accomplished either by enzymes, or by partial chemical hydrolysis, the polymer's cellulose backbone is readily biodegraded. Cellulose acetate is photo chemically degraded by UV wavelengths shorter than 280 nm, but has limited photo degradability in sunlight due to the lack of chromophores for absorbing ultraviolet light, and Cellulose acetate fibers in cigarette filters are designed to absorb vapors and accumulate particulate smoke components, Cellulose acetate [51, 52]Fig. 3.

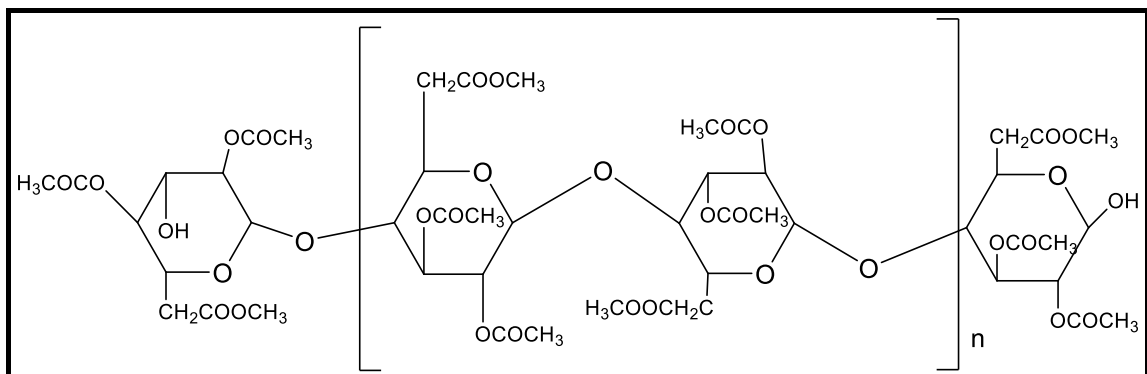


Figure3: Structure of cellulose triacetate, n is typically 400–1000 [52].

2.3.3 Zeolites

The first zeolite, called stilbite, was discovered by Cronstedt in 1756 who found that the mineral loses water rapidly on heating and thus seems to boil. The name "zeolite" comes from the Greek words zeo (to boil) and lithos

(stone) [53]. New zeolite composite membranes were synthesized using faujasite and cellulose membrane as precursor, two types of composites were prepared with different routes and characterized by Scanning electron microscopy, X-ray powder diffraction, Infrared spectroscopy, Raman and N₂ sorption. The composites were investigated in water treatment via ion exchange and filtration processes [54]. With the large surface area, natural zeolite could be used as excellent adsorbent for heavy metals adsorption. Moreover, wastewater could be treated at low cost because natural zeolites are cheap materials [55].

Zeolite is a potential adsorbent material for heavy metal adsorption. The ability of zeolites to adsorb and exchange ions is due to the cages and a negative charge of the zeolite. The cage and channel structure of zeolites are constructed by the aluminum and silicon atoms structure in three-dimensional framework of aluminosilicate tetrahedral, that are bound by the covalent bonds over common oxygen atoms in order to form interconnected cages and channel. Substitution of each Aluminum ion (Al^{3+}) with silicon ion (Si^{4+}) in the zeolite framework generates a negative charge in the zeolite. The negatively charge can be exchanged with heavy metal ions on the external surface of zeolite. However, the use of zeolite powder as an adsorbent remains challenging due to non-reusable adsorbent. An alternative method is by using support material incorporated with the zeolite. One of materials that can be used as a supporting material is polymer material, such as cellulose acetate in the form of membrane. CA is a polymer material

widely used as a membrane material. CA is an esteric polymer of hydrophilic acetic acid and cellulose. CA has several characteristics, such as high water absorption rate and heat resistance up to 60 °C[56].

2.3.4 Zeolitic Imidazolate framework (ZIF-L)

Recently a new zeolite imidazole framework named as ZIF-L was reported. The morphology of ZIF-L crystals is 2-dimensional leaf-shaped as shown in (Figure3a). ZIF-L has a cushion-shaped cavity between layers with a dimension of $9.4 \text{ \AA} \times 7.0 \text{ \AA} \times 5.3 \text{ \AA}$. The 2D layers stacking along the c direction are part of the sodalite (SOD) topology found in the 3D structure of ZIF-8 and there are six-membered ring and four-membered ring on them (Fig.4). The unique shape and pore systems of ZIF-L are very different from well-known MOF crystals[57].

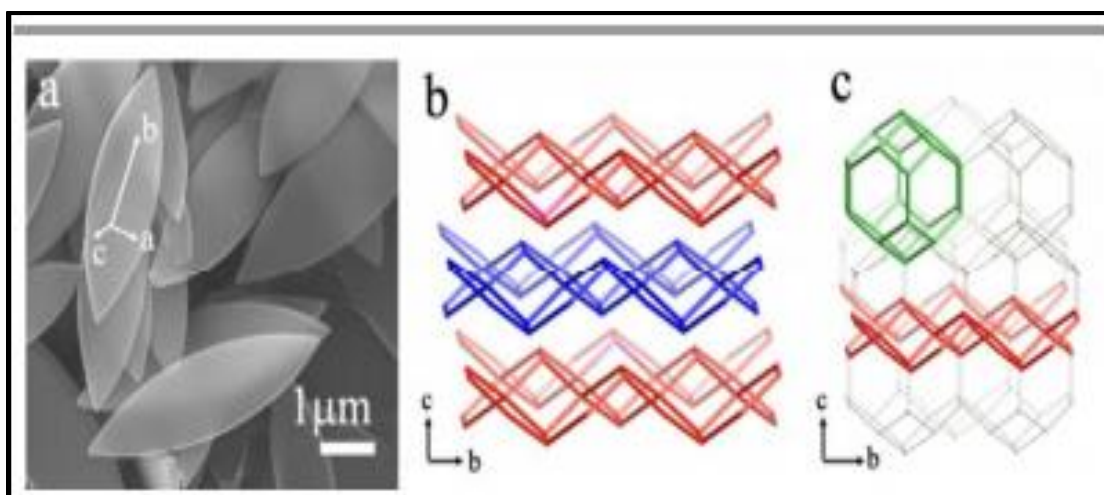


Figure 4: SEM image and crystal structure of ZIF-L [57]

Due to its 2D Nano flake structure, ZIF-L was fabricated on the porous carrier surface by vacuum filtration and used for removal of TC in

pharmaceutical wastewater [58-60]. Although ZIF films and/or membranes have been prepared on different substrates for separation and other applications, there has been no report on removal of TC from pharmaceutical wastewater by using ZIF-L film coated onto cellulose acetate.

Azeolitic imidazolate framework coated onto cellulose acetate film will be synthesized and used in the removal of TC from waste water. Zeolite composed of zinc (ZNF) Nanoflakes will synthesized from reacting zinc nitrate with 2-methylimidazole zinc then fabricated on the surface of cellulose acetate filter to form a 3-dimensional (3D) composite film. The film expected to be covered with coordination sites that binds TCA. The effect of various factors such as solution pH, contact time, temperature and solution concentration on adsorption efficiency will be evaluated. The film components and film will be subjected to various analytical, thermal and spectroscopic techniques.

2.3.5 CA/ZA Membrane morphology

Figure 5 shows that there is large number of zeolite dispersed uniformly in CA/ZA membrane as compared to the CA membrane. The dispersion of zeolite attributed by the silica and aluminum shown in Figure 5c and Figure 5d indicates that the zeolites were embedded in the cellulose acetate matrix. This is attributed to the interfacial interaction between zeolite and cellulose acetate [55].

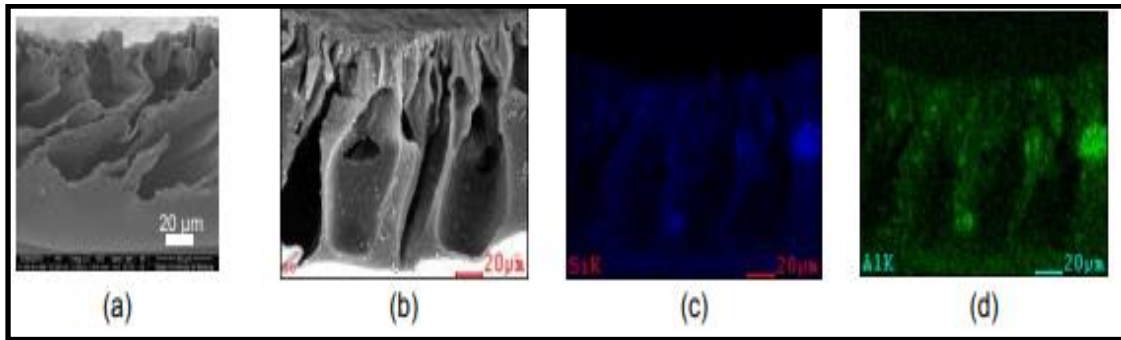


Figure 5: SEM images of cross section CA membrane(a), CA/ZA membrane(b), distribution of silica from zeolite (c), alumina from zeolite (d) [56].

2.4 Adsorption process

Understanding the adsorption process require accurate quantitative method to present the exact process occurs in adsorption and how are these materials behave in considering the isothermal, thermodynamic, and kinetic nature, with respect to isothermal study its meaning the adsorbed amount of a target analytes on the adsorbent as a function of its concentration in the solution at constant temperature. The adsorbed amount is always normalized because of the divided adsorbent mass, that effect allow precise comparison between different situations or compounds[61].

Adsorption equilibrium is confirmed when an adsorbate become in contact with the adsorbent for certain period of time, and in the presence of adsorbate concentration in the bulk solution that allows a dynamic equilibrium with the interface concentration.

In fact there is a wide parameters that influences the adsorption process that is in the solution chemistry like the initial concentration, PH, contact time, also the temperature can affect the adsorption reaction occur. Itis important

to analyze the isotherm data to fit it as an equation that exactly explains the observed behavior. The most known isotherms which are applied in liquid /solid systems are the theoretical equilibrium isotherm models, including Langmuir, Brunauer Emmett Teller (BET), Freundlich and Temkin isotherms, some of these models are shown next [62, 63], we were already fitted the data following Langmuir and Freundlich isotherm.

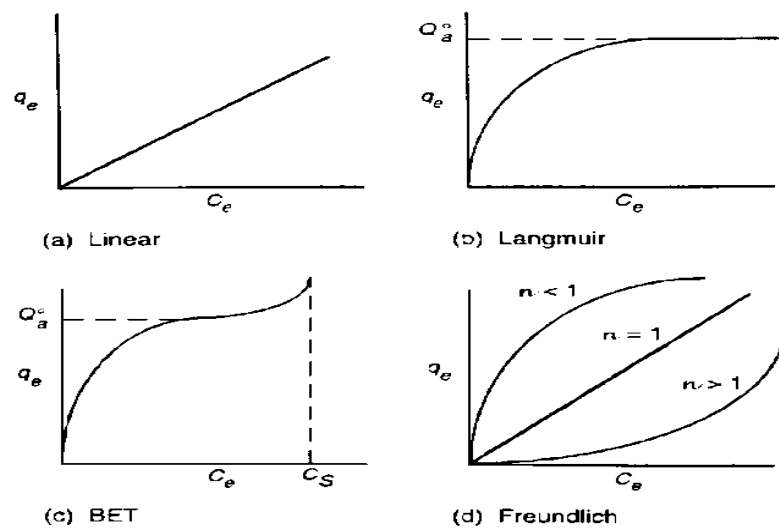


Figure 6: different adsorption isotherm models [62].

2.4.1 Langmuir Adsorption Isotherm

The outer surface of the adsorbent has a maximum capacity for adsorbate, so after the formation of a monolayer on this surface, no more adsorption occurs, so it is called "the ideal localized monolayer model"; such one was developed for representation of chemisorption process. In this adsorption, the process is limited to monolayer coverage, that's mean the adsorbed molecule cannot migrate across the surface into inner structure or interact

with neighboring molecules on other sites. Furthermore, the surface of the adsorbent is uniform, and so all the adsorption sites are energy equivalent[63].

The Langmuir principal relates the surrounding of molecules on a solid surface to the medium concentration above the solid surface at a constant known temperature and with fixed other parameters. This equation can be written as:

$$\frac{1}{q_e} = \frac{1}{q_0} + \frac{1}{q_0 K_L C_e}$$

Where:

C_e = adsorbate concentration at equilibrium (mg/L)

Q_0 = maximum capacity of monolayer coverage (mg/g)

K_L = Langmuir isotherm constant (L/mg).

A q_e is the adsorption amount of adsorbate per adsorbent unit mass (mg/g), and it can be calculated using the following relation:

$$q_e = (C_0 - C_e) \frac{V}{m}$$

Where:

C_0 is the initial adsorbate concentration in (mg/L).

V is the solution volume in (L).

And m is the adsorbent mass in (g).

$(C_0 - C_e)$ represents the adsorbed amount (ppm). We can derive the parameters of Langmuir by plot a values of (C_e/q_e) as a function of C_e in a graph, and the slope of such a graph represent $(1/q_0)$, while the y-intercept represent a $(1/K_L Q_0)$ [32].

The essential features of the Langmuir isotherm can be expressed in terms of a dimensionless constant separation factor R_L which is given by the following equation :

$$R_L = \frac{1}{1 + K_L C_0}$$

Where:

C_0 = initial concentration.

K_L = the constant related to the energy of adsorption (Langmuir Constant).

R_L value indicates the isotherm shape to be unfavorable if $(R_L > 1)$ Linear if $(R_L = 1)$, favorable if $(0 < R_L < 1)$, or irreversible if $(R_L = 0)$.

2.4.2 Freundlich Adsorption Isotherm

The adsorption process here depends on different affinities to heterogeneous surfaces. This isotherm model supposes that the bonds with stronger attractions with the surface available sites are occupied first and so on, as a result of increasing the occupied sites, the strength of binding reduced. Related to that articulation, the mass of adsorbate per mass of adsorbent can be calculated by the following equation [62-64].

$$\ln q_e = \ln K_F + \frac{1}{n} \ln C_e$$

Where:

K_F is a constant which indicates the capacity of the sorbent (mg/g).

n is a coefficient that gives an indication of the Favorable way of the adsorption process (g/L)ⁿ if the value of $1/n$ is less than one then the adsorption is normal, and if n is between one and 10, the sorption process is favorable [65, 66].

By plotting a values of $\ln q_e$ as y-axis with $\ln C_e$ as x-axis we can drive a parameters related to this type of isotherm, y-intercept represent $\ln K_F$ and the slope of the curve represent $(1/n)$.

2.5 Adsorption Kinetic Models

The kinetic energy for the process in physics represents the movement of an objects or in our case "target analyte" molecules from solution matrix to a close region of the solution in water around the adsorbent surface particle sites throw normal diffusion movement [67] this will represent by two way as following:

2.5.1 Pseudo 1stOrder Kinetics

This was the first model placed to describe kinetics energy for the adsorption reaction.

The rate for pseudo-1st-order kinetic model can be represented by the following equation:

$$\ln(q_e - q_t) = \ln q_e - K_1 t$$

Where: q_e and q_t are the amounts of target analyte that adsorbed per unit mass of adsorbent at equilibrium, and at time t respectively (mg/g). k_1 is the pseudo-1st-order rate constant for adsorption (min^{-1}). The rate constant K_1 and q_e can be calculated by plotting a values of $\ln(q_e - q_t)$ as y-axis versus values of t as x-axis.

2.5.2 Pseudo 2nd Order Kinetics

This type of kinetic assumes that the chemical adsorption is represent the rate determining step, which involves valence attraction between the adsorbate and the adsorbent by sharing or exchange of electrons.

The final integrated equation for this model type of kinetic is:

$$\frac{t}{q_t} = \frac{1}{K_2 q_e^2} = \frac{t}{q_e}$$

Here;

K_2 : adsorption pseudo-2nd-order rate constant ($\text{g.mg}^{-1}.\text{min}^{-1}$). By plotting a linear relation between the values of t/q_t as y-axis versus values of t as x-axis, we can drive $(1/ K_2 q_e^2)$ from y-intercept and $(1 /q_e)$ that equals the slope of the graph.

2.6 Adsorption Thermodynamics

Adsorption thermodynamics of a process are necessary to determine the nature of that process and whether the process is favorable or not[68]. The adsorption characteristics of a material can be expressed in terms of thermodynamic parameters as plotted into van 't Hoff equation to determine such parameters as the change in Gibbs free energy (ΔG), that give an information about how this process is favorable or not or how much is the spontaneity of this reactions, that's if the change in Gibbs free energy (ΔG) has a negative sign that mean its spontaneous process, the opposite is not spontaneous when it has a positive sign, also the Enthalpy change (ΔH) can be predicted quantitatively, and that indicate the associated energy needed or released by the reaction, there is also the change in Entropy (ΔS) indicating if the direct of the process toward more order or disorder side[69-71]. Here; ΔG and ΔH have a (J) unit while a ΔS has a unit of (J/K). The general relation which connects between the adsorption parameters will be written as[41]:

$$\Delta G = \Delta H - T \Delta S$$

With respect to ΔG , it can be also calculated using the following relation:

$$\Delta G = -R T \ln K_d$$

Whereas:

R: The Universal gas constant (8.314) J.mol⁻¹.K⁻¹.

K_D : Constant for thermodynamic equilibrium which equals (q_e/C_e) and has a unit of mole or (L/g). When equals the two equations that previously mentioned, that will result in the following relation:

$$\ln K_d = \frac{\Delta S}{R} - \frac{\Delta H}{RT}$$

By plotting a linear relation known as Van't Hoff plot between the values of $\ln K_d$ as y-axis versus the values of $(1/T)$ as x-axis, we can drive the values of $(\Delta S/R)$ that equals a y-intercept and $(-\Delta H/R)$ that equal a slope of the graph.

2.7 Analytical Techniques

Analytical method in general, should be suitable for the target analytes so it can be responded to its concentration at different value, for example in this type of research like in ERY we could not use UV-VIS spectrophotometer since it difficult to predict these very low concentrations at ppt scale and giving an acetated response sign, using this solid phase extraction, the adsorbate concentration at equilibrium, q_e (mg /g) is computed by the following equation:

$$q_e = \frac{C_0 - C_e}{W} V$$

Here C_0 , and C_e (mg/ L) are the adsorbate (ERY) concentration of initialization, and equilibrium and V (L) and W (g) are solution volume and adsorbent dosage, respectively.

The efficiency of the removal of ERY was calculated using:

$$\% \text{Removal} = \frac{C(o) - C(e)}{C(o)} * 100$$

Chapter Three

Experimental Part

3.1 Instrumentation

Instruments required in this work was: a bath of water shaker (Daihan Labtech, with variable speed 20 rpm to 250 rpm with speed control as digital), ultrasonic bath, pH scale meter (3510 model, JENWAY), thermometer scale, digital weighing balance (± 0.1 mg) . High Performance Liquid Chromatography - Shimadzu SCL-10A VP, using a SUPELCO Discovery reversed phase C18 column, (25 cm x 4.6 mm i.d., particle size 5 μm). The samples were injected manually through a Rheodyne injector. The wavelength of the UV/visible detector was fixed at 481 nm.

3.2 Chemicals and materials

The zeolite was acquired from NinghaiJiahe Chemical Industry Co. Ltd. (Zhejiang, China). The chemical composition of the zeolite was as follows (wt. %): $\text{SiO}_2 = 67.5$, $\text{Al}_2\text{O}_3 = 12.27$, $\text{CaO} = 3.29$, $\text{Na}_2\text{O} = 3.17$, $\text{MgO} = 0.47$, $\text{K}_2\text{O} = 1.54$, $\text{Fe}_2\text{O}_3 = 0.78$. The reagents, solvents and chemicals used in this study were documented with all their analytical specifications and their method of use as they were received without any modification. All reagents were purchased from Aldrich Chemical Company.

All solutions were prepared using distilled water. Cellulose acetate ($M_w = 30,000$ g/mol) was obtained from Shanghai Chemical Reagent Co. Ltd.

(Shanghai, China). Acetone was purchased from Guangzhou Chemical Reagent Co. Ltd. (Guangdong, China). Solution of erythromycin residue was taken from the sewage treatment plant, west of Nablus, and we made sure of the presence of the antibiotic erythromycin in it.

3.3 Methodology

3.3.1 Synthesis of cellulose acetate

Cellulose acetate will be prepared from reacting Nano crystalline cellulose with acetic anhydride in presence of sulfuric acid as a catalyst (Figure 7). Cellulose acetate then will be converted to a film by dissolving it in acetone and casting the solution in an evaporating dish[71].

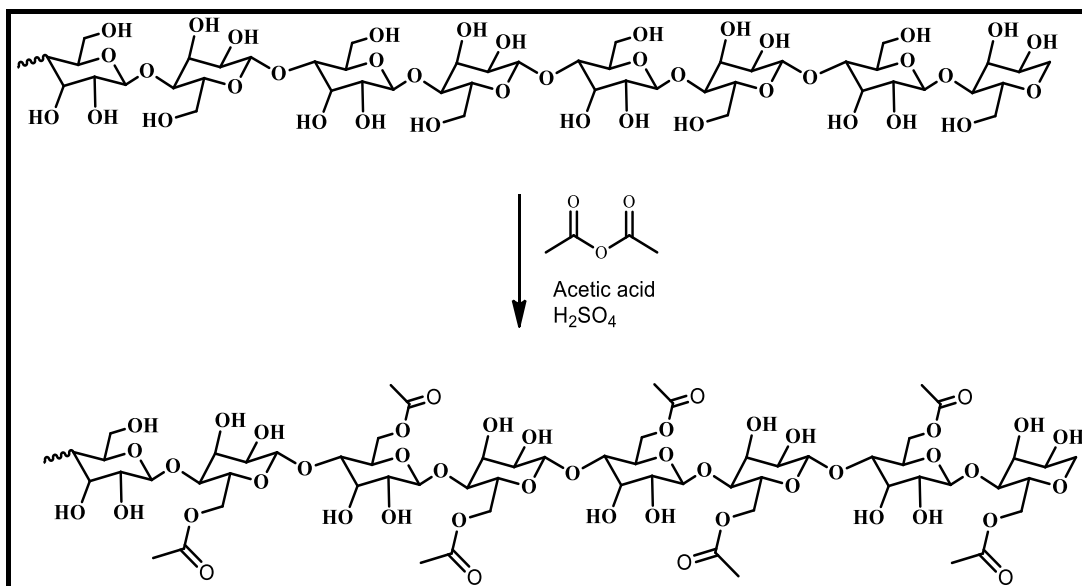


Figure 7: preparation of cellulose acetate [71]

3.3.2 Preparation of ZCAB fiber

The zeolite/cellulose acetate blend fiber (ZCA) was prepared by wet spinning process as follows: cellulose acetate (6 g) has been dissolved in 50 ml of acetone/water solution (6:1, w/w). The zeolite rocks were ground and sieved in order to have an overall dimension of around 800 mesh.

1.5 g of zeolite particles is added to the solution and scattered by mechanical stirring. The blended solution was pushed into a stainless-steel spinner and then protruded into a water coagulation bath to create a solid filament. The fiber was removed from the bath and cleaned twice with purified water. Finally, the fiber was dried at 30°C and sliced into very small fragments [72].

3.3.3 Characterization of ZCAB fiber

The morphology of ZCA fiber has been analyzed by electron scanning microscopy (SEM) on the electron probe micro analyzer (Hitachi S-4700, Japan). ZCA fiber was snapped in a liquid nitrogen atmosphere to create an unpolluted cross-section for cross-section scanning.

The crystal structure of the fiber was characterized by the Philips X'pert PRO X-Ray diffractometer (XRD-Shimadzu XD-D1) with the mono chromatized graphite Cu-K alpha (15418 Å) radiation source at a scanning speed of 20°/min. Scanning electron microscopy (SEM) micrographs have been studied using a Carl Zeiss field emission scanning electron microscope for surface and cross-section morphology of the prepared filament. The Fourier Transform Infrared (FTIR) fiber spectrum was obtained using the Bruker

Alpha-P spectrophotometer. FT-IR spectra were reported from 400 cm^{-1} to 4000 cm^{-1} with 32 scans on Nicolet NEXUS-470 FT-IR (America) apparatus and a resolution of 4 cm^{-1} . [73]

Shimadzu UV 1800 UV-Vis spectrophotometer with UV probe program was used to test the absorption spectrum of the sample. The ERY concentration was determined by quantitative examination of the UV-Vis spectrophotometer (SHIMADZU, UV- 1201). ERY solution was measured at 481.5 nm, the wavelength that the ERY gives the highest absorbance.

X-ray diffraction was performed using CuK Al radiation on the Panalytical X'Pert Pro diffractometer (1.5418 \AA) from 2° to 70° (2θ) at a scanning rate of 1° per min. Membrane porosity was also measured using the water intrusion method [73, 74].

Thermogravimetric analysis was carried out on DTG 60H equipment (Shimadzu Co., Japan). Around 3.0 mg of adsorbents were heated from 25°C to 700°C in the nitrogen atmosphere (50 mL/min) at a temperature of $10\text{ }^\circ\text{C/min}$. Decomposition temperatures of the compounds were derived from the first mass loss (percent) versus temperature derivative (DTGA) [75, 76].

3.4 Calibration Curves

Commercial 95.1% erythromycin $733.937(\text{g/mole})$ was used to prepare 1 L of 1000 ppm stock solution by dissolving exactly $854\text{ }\mu\text{L}$ using micropipette into 1000 ml volumetric flask completing the volume to the mark with 50/50 acetonitrile: distilled water solvent. Then the stock solution was diluted to

prepare a series of several standard solutions of ERY by using the following relation for dilution calculations ($M1*V1 = M2*V2$). The prepared initial concentration of ERY was (5, 10, 15, 30, and 50 ppm). As in figure 8 prepared standard solutions were used then in our batch experiments to study the effect of different parameters that affecting adsorption process such as time, PH, and temperature and hence to predict the optimum conditions for efficient adsorption reaction for ERY with Zeolite/Cellulose Acetate (ZCA) in blend fiber

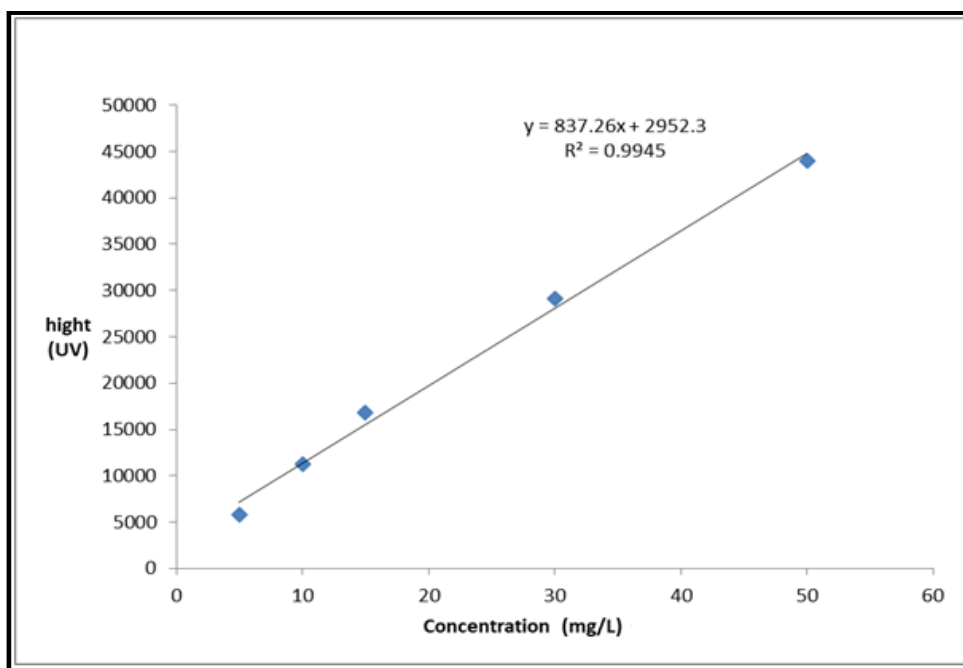


Figure 8: calibration curve for ERY standard solution using UV instrument.

UV was used to construct the calibration curve through measuring the high of the peak of ERY chromatogram. According to Beer-Lambert law, solutions with high concentration absorb more light than solution of lower concentration, since concentration and absorbance are directly proportional. So this law can be used to determine an unknown concentration depending on using the calibration curve of standard solutions of the same material.

3.5 Batch Adsorption Experiments

This research follows batch experiment procedure that each steps done alone in vials with no flowing of analyte or contaminated water through a constant adsorbent column, whereas the other type of adsorption procedure is the continuous technique in such process the water was polluted by containing adsorbate comes through a column that contains a fixed adsorbent, and the amount of adsorbate that enters is highly depends on the flow rate of solution. Here in our batch technique, adsorption process were highly affected by several other factors influencing the adsorption efficiency, the most important is that the adsorbate and adsorbent dose, time of shaking, pH value of the solution and temperature, so each those parameters were studied and each optimum parameter was taken in account for next experiment.

ERY concentrations was determined in the filtrate by UV-Vis spectrophotometer at 481 nm through the concentration of its derivatives. The batch kinetic studies conducted were identical to the adsorption experiments, but the aqueous samples were taken at pre-specified time intervals. The amount of ERY adsorbed at time (t) was calculated by mass balance equation. The absorbance of the solution was recorded by UV-Vis spectrophotometer instrument at a wavelength of 481nm and the ERY concentration which adsorbed/removed was determined via following equations:

$$Q_e = (C_o - C_e) / m V$$

$$R\% = (C_o - C_e) / C_o \times 100$$

Where q_e is the amount ($\text{mg}\cdot\text{g}^{-1}$) adsorbed and $R\%$ is adsorption efficiency. The effect of solution conditions including amount of prepared polymer, time, temperature, pH value and toxic metal ion initial concentration were studied. Atomic adsorption measurements of the filtered mixture were made for each sample to calculate the residual concentration of the ERY and thus to evaluate the efficiency of the adsorption.

3.5.1 Effect of contact time

To reach the equilibrium state in the adsorption process, the time required to fill out the available site on the adsorbent and thus no more adsorption occur is called contact time, it's very important to predict the optimum time that is exactly needed to reach the reaction equilibrium and at the same time not more than needed. the adsorption amount ERY, was studied and instrumentally predicted after time interval in order to predict the optimum required time of shaking for the adsorption process, the experiments were done at room temperature 25°C where a constant volume of 10 ml (15 ppm) standard solution was shaken with 1 mg of adsorbent solution, and at the end of time interval (5 min to 1h) the concentration of the remained ERY was measured using UV.

3.5.2 Effect of PH

The adsorption process is highly affected by the amount of H_3O^+ and OH^- ion in the solution that's mean the effect of pH value is very important factor to study and control, since these ions can attached on the adsorption site of adsorbent surface changing its behavior and affinity toward the target analyte

by either reducing or increasing the adsorbed amount and then get more or less efficient process, so that the effect of pH value on the adsorption reaction was studied over a wide range of pH value ranging from 2 to 7 to predict the value at which the adsorption reaction is more efficient, the percent of removal was plotted as a function of pH. The initial pH for the solutions of ERY before any modifying was nearly 5 and a roughly prepared concentrations of 0.1 M HCl and 0.1 M NaOH solutions was used to adjusting the pH value of ERY solutions before the addition of adsorbent.

The adsorbent samples (1 mg of each) were added to 10 ml of the prepared standard solution of constant 15 ppm concentration. The prepared combination solutions were placed in shaking water bath at room temperature (25°C) for a period of optimum contact time that is already measured for each previous adsorption process.

3.5.3 Effect of temperature

The direction of the heat flow between the system and its surrounding is important to predict the type of our reactions or processes if it's either endothermic process (positive enthalpy) or exothermic process (negative enthalpy) so it's very important to prepare a good thermal conditions to have a good percent of removal for analyte, that were done by study the effect of temperature on removal efficiency and also, the obtained data can be used to calculate van 't Hoff parameters to understand the reaction nature of spontaneity and energy needed or released. So that to study the effect of

solutions temperature on the adsorption process, 10 ml of 15 ppm standard solution of ERY was transferred into vials with adjusting its PH to the optimum value that were predicted previously for each one.

The solutions were placed in shaking water bath at desired temperature (the range was 20°C to 45°C), then the adsorbent (1 mg) was added to it for optimum contact time. After the time is over the samples were filtered and the adsorbate amount was determined by UV instrument, the data obtained was a percent as a function of temperature.

3.5.4 Effect of adsorbent dose

The affinity of each solute to dissolve in different layer is varied depending on its physical and chemical properties, knowing that adsorbent have a limited adsorption site for interact with solutes, moreover the total amount of adsorption site will increase with increasing the adsorbent dose, any way there is some unabsorbed amount of analyte that will stay soluble in solutions at extremely low quantity (about 1%), however any further addition of adsorbent will be unnecessary and wasted, and it's really important to predict the exact required amount of adsorbent to satisfy a highest % removal at the same time no wasted material. In order to find out the optimum amount of adsorbent that is required for the adsorption of ERY on ZCAF, a (5, 10, 15, 30, and 50) mg of adsorbent was added to five vials each containing 10 ml of 30 ppm of ERY solution. The mixtures were placed in shaking water bath for optimum contact time for each case at either 35°C or 25°C with modifying (pH=7). The mixture shaken also for optimum time at 25°C with neutral pH.

The concentration of ERY in the filtrate was measured using UV.

3.6 Computational and Theoretical Study

The geometry optimization of the ERY was performed by G09W [77] with Hartree-Fock[78, 79] method and 6-311G** [80, 81] basis set in the gas phase. In theoretical predictions of the chemical reactivity, the Koopmans' theorem [82] is the first essential step to calculate the ionization energy (I) and electron affinity (A) values via the FMO energies

$$I = -E_{\text{HOMO}}$$

$$A = -E_{\text{LUMO}}$$

Moreover, the quantum chemical parameters (QCP) [83-86], which are defined as χ "electronic chemical potential", η "global hardness", ω "electrophilicity index", ΔN "fractional number of the electrons transferred" in case of B and C systems have contacted each other, and ΔN_{max} "maximum charge transfer capability", have been also obtained from the I and A values with using the following formulae

$$\chi = -\frac{I + A}{2}$$

$$\eta = \frac{I - A}{2}$$

$$\omega = \frac{\mu^2}{2\eta}$$

$$\Delta N = \frac{\chi_C - \chi_B}{2(\eta_C + \eta_B)}$$

$$\Delta N_{\text{max}} = \frac{I + A}{2(I - A)}$$

In addition, Gazquez and co-workers introduced two useful parameters to calculate the ω^- “the electro donating power” and ω^+ “the electro accepting power” parameters [87]

$$\omega^+ \approx (I + 3A)^2 / (16(I - A))$$

$$\omega^- \approx (3I + A)^2 / (16(I - A))$$

Also, the $\Delta E_{\text{back-donation}}$ “back-donation energy” [88] is a powerful value and defined as the following equation,

$$\Delta E_{\text{back-donation}} = -\frac{\eta}{4}$$

In addition, the stabilization energy lowering obtained from the second-order perturbative energy analyses depending on the NBOs “Natural Bond Orbitals” [89-91] is defined as

$$E^{(2)} = \Delta E_{ij} = qi \frac{(Fij)^2}{(\epsilon_j - \epsilon_i)}$$

For the molecular system, qi states the donor orbital occupancy, ϵ_i , and ϵ_j are diagonal elements, and Fij is the off-diagonal NBO Fock matrix element where “ i ” and “ j ” are the filled and unfilled molecular orbitals.

Chapter Four

Results and Discussion

4.1 Adsorbent characterization results (BET)

Nitrogen adsorption–desorption isotherms were measured at -196°C on a Quantachrome Autosorb AS-1 instrument (USA). BET specific surface area of ZCA was calculated by using the nitrogen adsorption isotherm data at low temperature [92] based on the adsorption data at P/P_0 of 0.05 - 0.2. and it was determined as $2.47\text{ m}^2/\text{g}$. Pore volume and average pore size were computed by BJH model [93]. The pore volume of ZCA sample was determined as $2.45 \times 10^{-2}\text{ cm}^3/\text{g}$ and pore diameter was 3.5 nm. According to the standards prescribed by the Pure and Applied Chemistry International Union (IUPAC), the materials with pore diameters between 2-50 nm are classified as mesoporous materials [93]. As Result ZCA can be regarded as a mesoporous material.

4.1.2 Characterization of ZCA fiber using SEM

The morphology of ZCA fiber has been observed by SEM. figure9 demonstrates the surface morphologies and cross-section configurations of the ZCA filament. As seen in figure7, the surface of the ZCA fiber is comparatively smooth and the diameter of the as-prepared fiber is approximately 250 nm. The sponge-like shape of the ZCA fiber is observed, as seen in the cross-section. The ZCA fiber has a homogeneous, extremely

porous composition. Zeolite crystals, which are about 100 μm in size, are embedded in the ZCA fiber network. As can be seen in Fig. 9, cellulose acetate serves as a support for the matrix and the pore size of the fiber is between 5 and 10 μm . For interaction with the adsorptive sites of the ZCA particles, ERY could rapidly diffuse into the pores.

The dispersion of zeolite attributed by the silica and aluminum shown in Fig. 9b and Fig. 9c indicates that the zeolites were embedded in the cellulose acetate matrix. This is attributed to the interfacial interaction between zeolite and cellulose acetate.

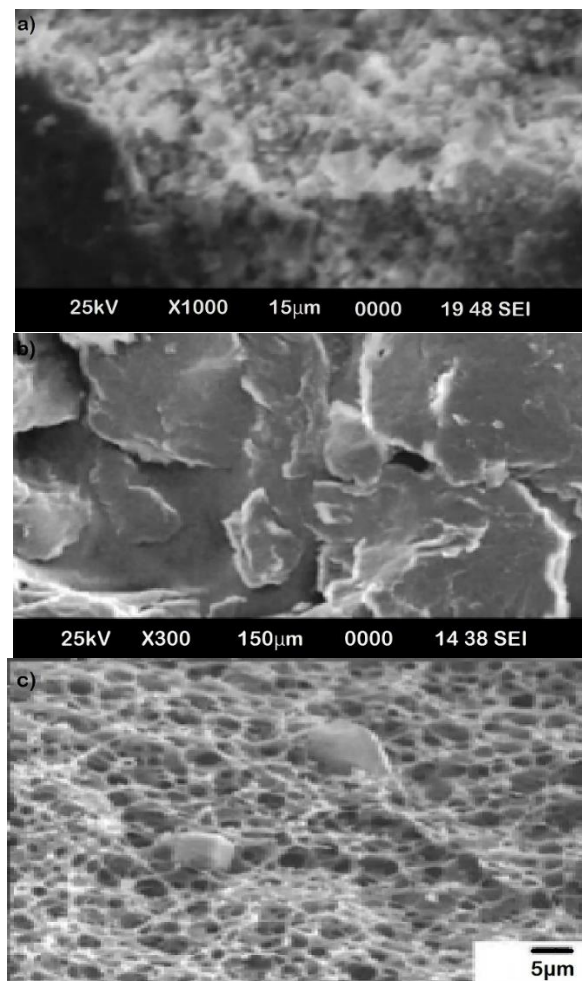


Figure 9: SEM images of (a) ZCA fiber b) Zeolite c) cellulose acetate (CA).

4.1.3 X-ray diffraction analysis

Fig. 10 shows that the diffractogram of the synthesized zeolite is similar to JCPDS No. PDF 0038-0241 for LTA type zeolite-A [$\text{Na}_{96}(\text{AlO}_2)_{96}(\text{SiO}_2)_{96} \cdot 216\text{H}_2\text{O}$]. Furthermore, diffractogram of CA as shown in the figure, appropriates with a diffractogram reported by Fan et al. (2013) [94], who stated that CA has distinctive angles at 2θ of 10° and 13.2° . These two typical angles were also recognized as the crystalline peaks of modified CTA II (Deus et al., 1992). In addition, Jayalakshmi et al. (2014) reported that the diffractogram of CA membrane had a typical semi crystalline angle at 2θ of 9.6° and two crystalline angles at diffraction angles of 20.1° and 26.8° .

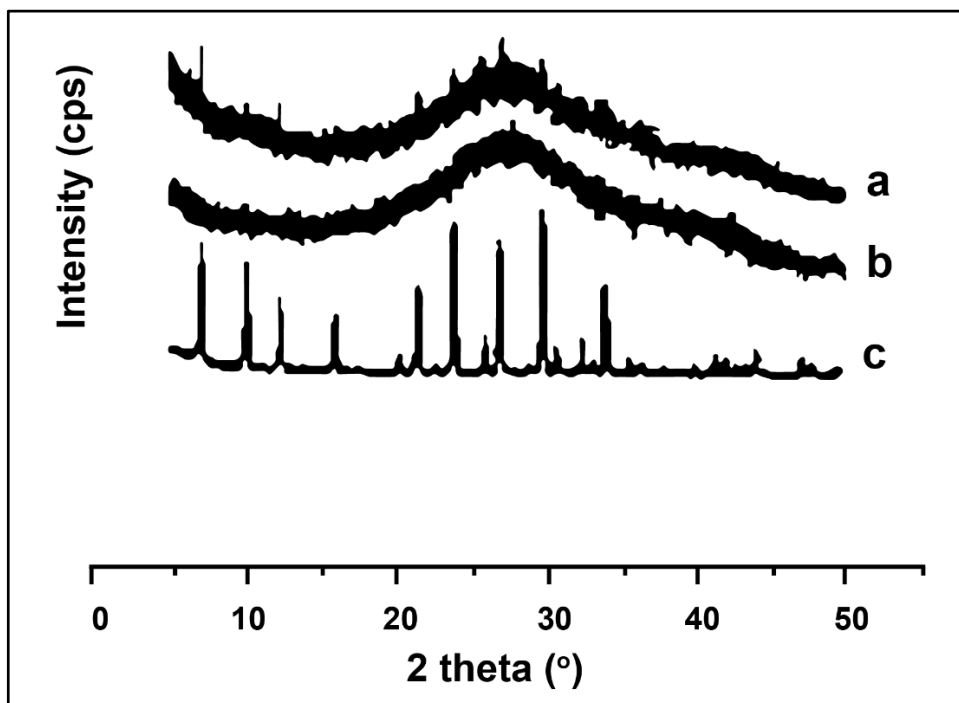


Figure10: Comparison of X-ray Diffractograms of: (a) Zeolite, (b) CA and (c)ZCA.

The diffractogram of CA membrane in this study were identified as a crystalline peak at 26.8° . Composite membrane also has a crystalline peak at 26.8° . Moreover, the composite membrane has also a weak peak at 10° and 13.2° indicating the typical peak of CA in different intensities. It was caused by a decreasing crystallinity form in the membrane compared to CA solids. It was reviewed that the CA/ZA membrane has a peak at an angle of 10.3, 12.6 and 16.2 indicating the presence of zeolite-A. Based on the results of the composite membrane diffractograms, it was known that zeolite-A has better dispersity in the CA porous membrane as a filler.

4.1.4 FT-IR analysis

Fig. 11 demonstrates the ZCA fiber FTIR spectrum before and after ERY adsorption. As can be seen, a peak of $600\text{-}800\text{ cm}^{-1}$ was observed, which is associated with T-O-T stretching and T-O zeolite bending [95]. A sharp peak in such region indicates the presence of zeolite inside the membrane. In addition, the membrane showed a peak in the region of $1,000\text{-}1,200\text{ cm}^{-1}$, indicating the interaction between Si-O-Si of zeolite and CA.

Some peaks were also detected at $1,735\text{-}1,738\text{ cm}^{-1}$ assigned to carbonyl C=O stretching of CA and broad peak at about $3,400\text{ cm}^{-1}$ assigned to O-H stretching. Furthermore, the absence of new peaks was observed on the membrane after the adsorption process. However, the peak was slightly shifted and the peak intensity decreased. This might be due to the presence

of Van der Waals force, indicating the physical adsorption between the metal ions and membrane.

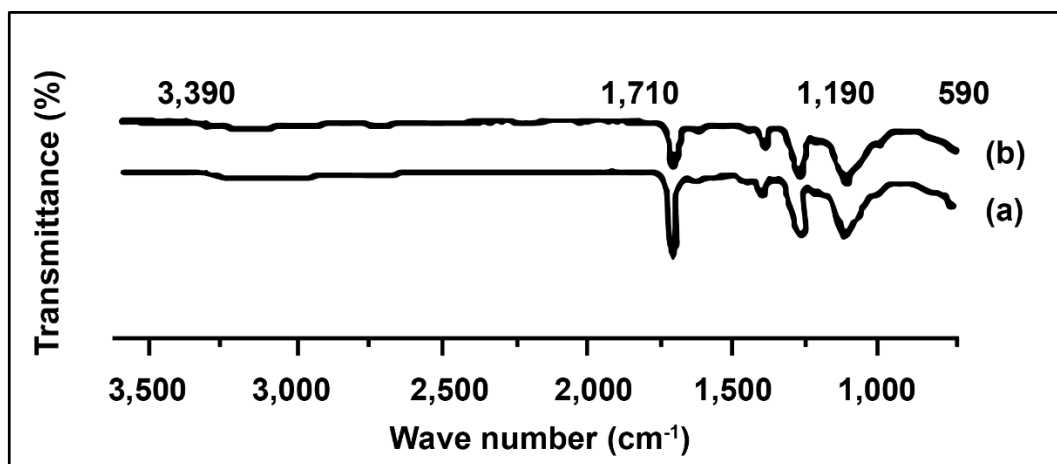


Figure11: FT-IR for ZCA a) before adsorption and b) after adsorption process of ERY.

4.1.5. Thermo gravimetric analysis (TGA).

Fig. 12 indicates the TGA curve for zeolite, cellulose acetate and ZCA material. According to the TGA thermogram obtained for cellulose acetate (CA), there is initially a minor weight loss of 3% to 200°C, leading to the loss of volatile compounds and H₂O bound to the hydrophilic (OH) groups of the CA chains and, consequently, to CA deacetylation[96].

Here were two more steps of thermal decomposition of this material; the first phase was between 300 and 400°C , with a weight loss of 79 percent, and the second was between 400 and 600°C, with a weight loss of 14 percent. The first stage (300 – 400°C) refers to the major thermal decomposition event which can be traced to the degradation of the CA. The final stage of mass

loss (400–600°C) is attributed to complete degradation and decomposition of the film [96].

Two levels of mass reduction have been found for zeolite. The first stage was between 30 and 230°C, with a weight loss of 40 percent which can be due to the loss of H₂O adsorbed to the material and to the deterioration of certain aluminum and silicate fractions which did not decompose at 400°C during the pyrolysis process. The second stage of zeolite thermal decomposition, beginning at 380°C, which can be assigned to the release of minerals and salts from the material corresponded to approximately 35% of its initial mass, indicating its high mineral residue content.

From the ZCA fiber thermogram, we observed three levels of thermal decomposition between 30–200°C, 215–380°C and above 380°C. This thermogram revealed an intermediate profile in comparison to the CA and zeolite thermograms, i.e., for both of the temperature scales of the thermal events referred to above, their mass variations occurred roughly as the sum of the other two thermograms, because the fiber is made up by 50 percent of the weight of each part. The first process, with a weight loss of approximately 20%, can be attributed mainly to the release of H₂O from the material due to the presence of zeolite, the CA mass being practically constant in this temperature range. The second stage of decomposition is probably due to the degradation of the CA chain, with the zeolite mass remaining almost unchanged. The CA mass loss at this stage was 80 percent. The third and final stage can be due complete fiber degradation and part of

the fiber has thermal stability lower than CA with maximum CA losses at 335 and 360°C, respectively.

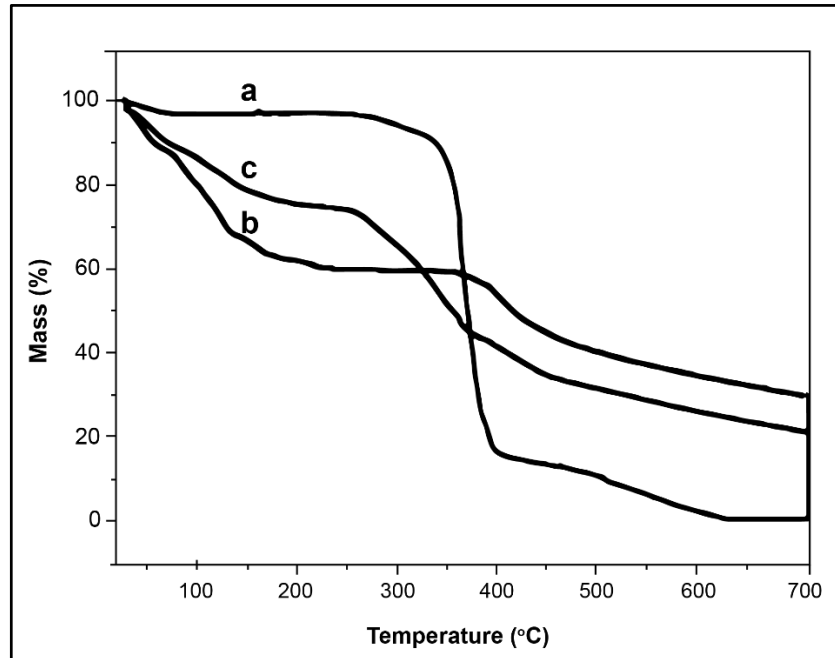


Figure12: Thermogravimetric analysis (TGA) for (a) Zeolite\CA(ZCA), (b) CA and (c) zeolite.

4.1.6. Differential scanning calorimetry (DSC).

The DSC thermograms obtained for CA and ZCA had identical profiles; the major difference was the initial temperature, peak and final melting temperature, as well as the enthalpy involved in this process, as seen in Fig. 6. The initial, peak and final temperatures for CA were 210, 211 and 216 °C, respectively, while those for ZCA were 190, 192 and 204, respectively. Whereas for ZCA were 190, 192 and 204 °C, respectively. While those for ZCA were 190, 192 and 204°C respectively, while those for ZCA were 190, 192 and 204°C respectively. ZCA melting happened at a temperature lower than that of CA melting. This may be attributed to a strengthening as well as

a lower amount of contacts between the CA chains. The melting enthalpy was 660 kJ/g for CA while it was 3600 kJ/g for ZCA. The higher energy involved during the ZCA melting process may be due to water volatilization, since TGA showed large mass loss in this temperature range.

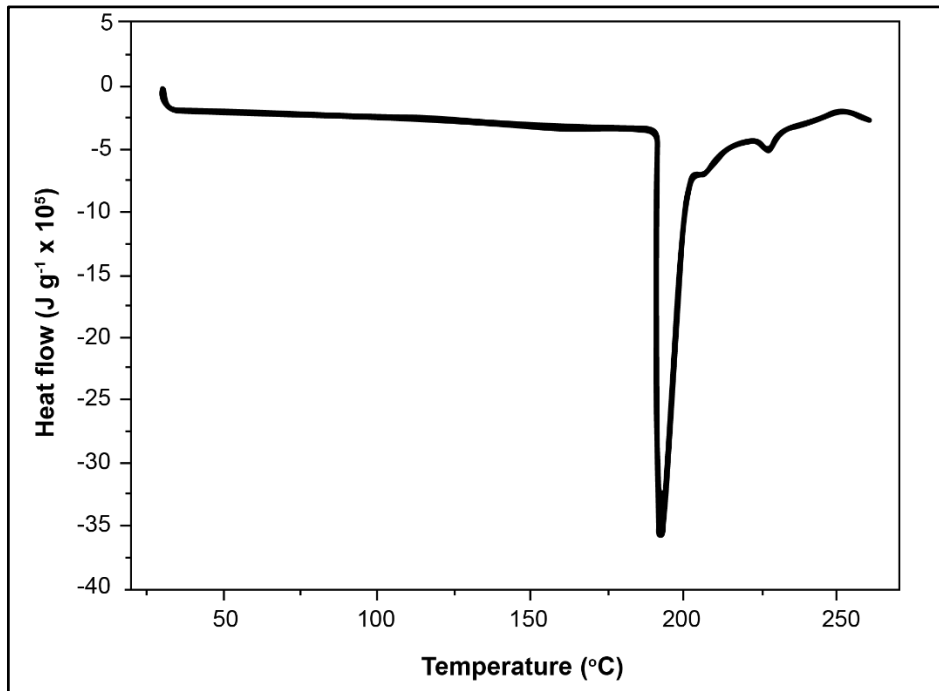


Figure13: Differential scanning calorimetry (DSC) for cellulose acetate film (CA) and cellulose acetate/Zeolite (ZCA).

4.2 Results of Adsorption

This research aims to use Cellulose Acetate (CA) in blend fiber for adsorption of erythromycin residue from pharmaceutical wastewater, and to compare the adsorption efficiency of the prepared polymers. After finding the remaining concentrations, the percentage of removal must be determined for each uptake. This value is defined as the ratio of the difference in the concentration of adsorbate before and after adsorption ($C_i - C_f$), to the initial

concentration of the ERY in the aqueous solution (C_i), as shown in the following equation:

$$\% \text{Removal} = \frac{C(i) - C(f)}{C(i)} * 100$$

Where;

C_i : Initial concentration of ERY in solution (ppm).

C_f : Final concentrations of ERY in solution (ppm).

The effect of solution conditions like temperature, PH, contact time, adsorbent dose, and initial concentration for the adsorption of ERY on acetate (ZCA) in blend fiber adsorbent was determined. The efficiency of the adsorption was raised up despite that it took more time to reach the equilibrium and maximum absorptivity.

4.2.1 Effect of contact time

The time required between adsorbent and adsorbate to allow the direct and dynamic contact for saturation state. It's important to predict the time of contact that required to achieving optimum removal, that give us an information about the kinetic of the adsorption reaction occur and how fast the process, that was done by dissolving 1 mg of adsorbent in 10 ml of 15 ppm initial concentration of ERY solution with no PH modifying at room temperature then taking a sample to analyzed each period of time (5, 10,15, 20, 30, 50, 60, 90,120) min, the measurement were done in triplicate trial on UV instrument.

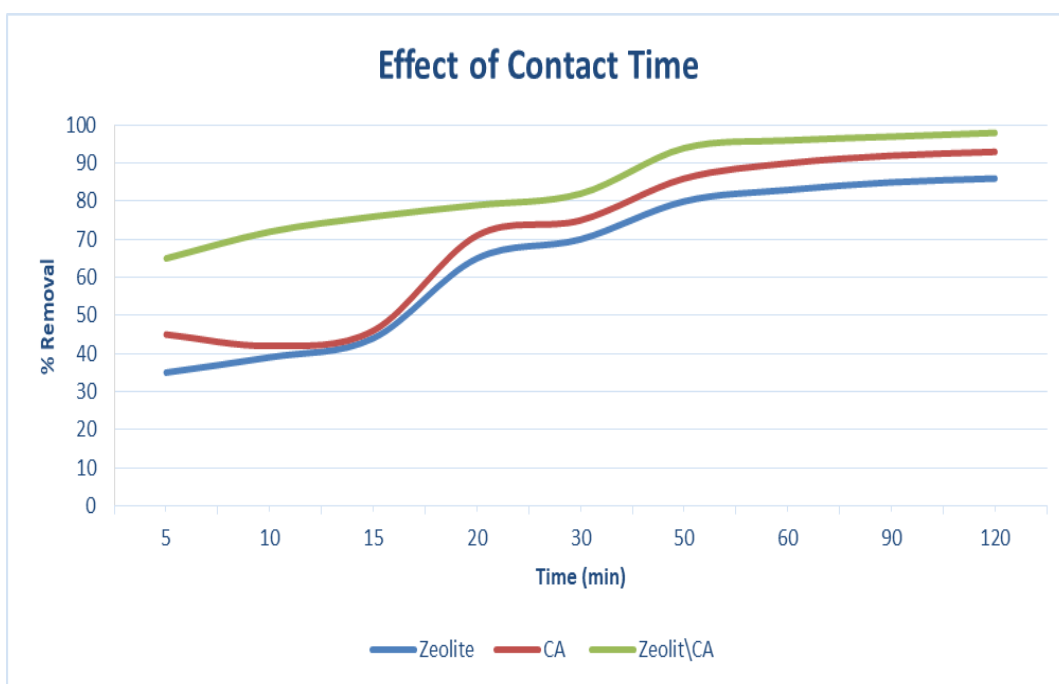


Figure 14: effect of contact time on the removal of ERY using ZCAB.

The effect of the time on the adsorption efficiency was studied at room temperature (25 °C), an initial concentration of ERY of 15 mg.L⁻¹, at different time intervals; 5, 10, 15, 20, 30, 50, 60, 90 and 120 min as shown in Figure 14. The adsorption of ERY onto the surface of the adsorbents was rapidly increased in the early stage (5, 10, 15, 20, 30) min (, due to the high number of active sites; and then the adsorption was increased slowly. This graph shows that the highest percentage of ERY removal was for ZCA after 50 minutes of shaking as the optimum contact time between adsorbent and adsorbate, and this percentage is approximately 94.0%.

No observable adsorptions were monitored after time intervals, including 50 to 120 min, this fact proves that the complex derivatives generated in the initial adsorption stage are unstable, leading to faster adsorption rate. The next slower adsorption rates could be ascribed to sapping the driving force

to result in decreasing the existing adsorption sites. The different adsorption efficiencies proved that the adsorbents did not exhibit similar morphologies.

4.2.2 Effect of temperature

To study the effect of temperature on the removal efficiency of ERY using ZCAB, the optimum conditions for other parameters was taken in consideration. In general, the, the adsorption efficiency becomes higher when increasing temperature values. The adsorption measurements were performed using an adsorbent weight of 20 mg, an initial concentration of 10 mg/L, and time interval at 30 min. With increasing the temperature from 20 °C to 45 °C.

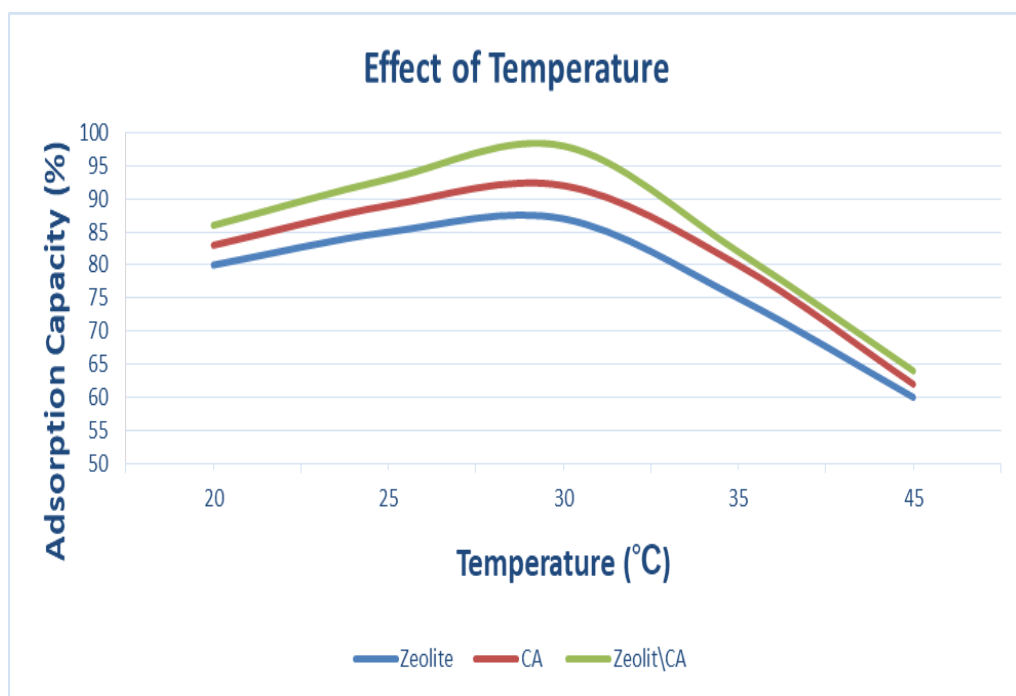


Figure15: effect of temperature on the removal of ERY using ZCAB.

As shown in the graph, the adsorption of ERY on a ZCAB increased as temperatures rose from 20 to 30 then the efficiency of removal decreased

from 30 °C to 45 °C with farther heating for the solutions, such that the percentage removal of ERY at the optimum temperature was 98%, increasing the adsorption efficiency, that indicating endothermic process, This could be attributed to increasing removal rate of ERY, with increasing the temperature, throughout the porous structure of the ZCAB ,The adsorption process may include both physical and chemical adsorption due to high temperature. Thus, the endothermic adsorption process could be ascribed to increasing the pore diameter and surface activation.

4.2.3 Effect of Adsorbate Initial Concentration

The adsorbent has a maximum adsorption amount for the analyte or adsorbate due to its limited adsorption sites on its surface, there is a suitable initial concentration to start with, to achieve the optimum removal as a high % of removal by plotting it as a function of initial concentration of ERY as shown in the graph.

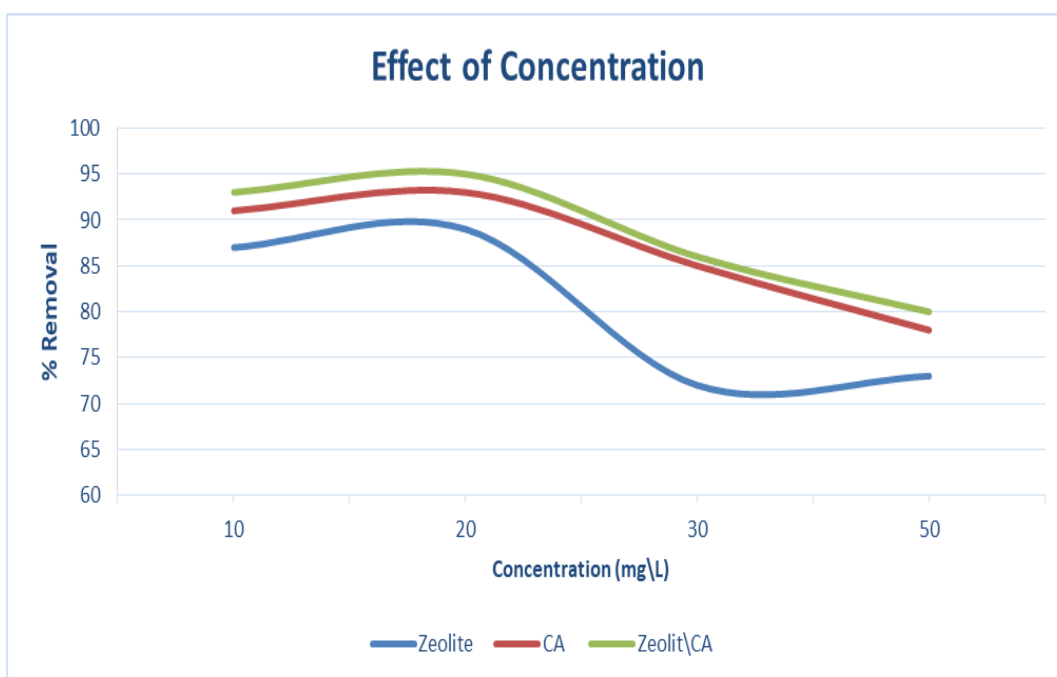


Figure16: Effect of initial concentration on the adsorption of ERY on to ZCAB

This was done by taking a 10 ml of 4 different initial concentrations of ERY standard solution (10, 20, 30, and 50) ppm treated with a constant adsorbent dose for 30 min, at 30°C. As the initial concentration increased from 10 ppm to 20 ppm the % removal was increased. The maximum removal was taken as 95% at the initial concentration of 20 ppm while it was just 80-86 % for 30-50 ppm solution.

As seen in Table 3, with reference to previous studies. The innovation of this study can be summarized as using zeolite/cellulose acetate blended fiber as the first example in the ERY removal literature.

Table 3: Previous studies on ERY removal from water

Adsorbent	Optimum Condition	Percentage removal (%) or adsorption capacity (q_m)	Reference
magnetic activated carbon	Initial ERY concentration of 65 mg L^{-1} , sorbent weight of 1.55 g L^{-1} , the contact time of 76.25 min, and at the temperature of $35 \text{ }^\circ\text{C}$.	95.125%	[32]
Magnetic imprinted polymers (MIPs) from chitosan	Initial ERY concentration of 10 mg L^{-1} , and at the temperature of $25 \text{ }^\circ\text{C}$. pH=4	Adsorption capacity (q_m) = $52.32 \text{ } \mu\text{mol/g}$ at $15 \text{ }^\circ\text{C}$.	[16]
Multi-Walled Carbon Nanotubes	mixing rate of 200 rpm, amount of adsorbent up to 1 g/L , and at the temperature of $75 \text{ }^\circ\text{C}$	99.4%	[97]
porous magnetic graphene (PMG)	pH of 3, contact time of 30 min, initial antibiotic concentration of 200 mg/L , and adsorbent dose of 0.35 g/L .	adsorption capacity (q_m)= 286 mg/g .	[98]
Fe_3O_4 /activated carbon/chitosan (MACC: Magnetic activated carbon/chitosan)	15 mg adsorbent, and at the temperature of $20 \text{ }^\circ\text{C}$	adsorption capacity (q_m)= 526.31 mg/g	[99]

Amberlite XAD-4	0.002 mg adsorbent at 30 °C	adsorption capacity (q_m)= 358 mg/g	[100]
zeolite/cellulose acetate blend fiber (Our study)	Initial ERY concentration of 20mg L ⁻¹ , the contact time of 60 min, and at the temperature of 30 °C.	98%	

4.3 Equilibrium Isotherm Models

The Langmuir and Freundlich isotherm are the two most widely used models to represent equilibrium data of adsorption of ERY onto three adsorbents were investigated at 25 °C for 30 min, with an adsorbent weight of 30mg/L (Fig. 17).

Equilibrium study was carried out in order to understand the mechanism of adsorption process, i.e., Langmuir [101] and Freundlich [92], which assumes the adsorption of adsorbate as a function of equilibrium concentration. Langmuir isotherm best describes the monolayer adsorption of solute from solution onto adsorbent surface having finite number of active sites present on it. The results of the models are shown in Table 4. A dimensionless constant R_L was calculated using the next equation.

$$R_L = \frac{1}{(1 + K_L C_o)}$$

Where C_o is the original concentration of ERY (mg/L) and where K_L is the constant of Langmuir isotherm. The R_L value represents adsorption mechanisms that are unfavorable ($R_L > 1$), linear ($R_L = 1$), desirable ($1 > R_L > 0$) or irreversible ($R_L = 0$) [96]. The R_L (0.106) values for ERY in the

present study was <1 for the three adsorbents, which indicated favorable adsorption. Freundlich isotherm considers the heterogeneous surface and non-uniform distribution of heat of sorption. It is most favorably studied for description of multilayer adsorption process.

In particular, Isotherms were best suited to Langmuir models, which may be due to the high regression coefficient (R^2) value (Table4). It can also be observed that the surfaces of all three adsorbents are homogeneous and that adsorption occurred mainly in the monolayer system.

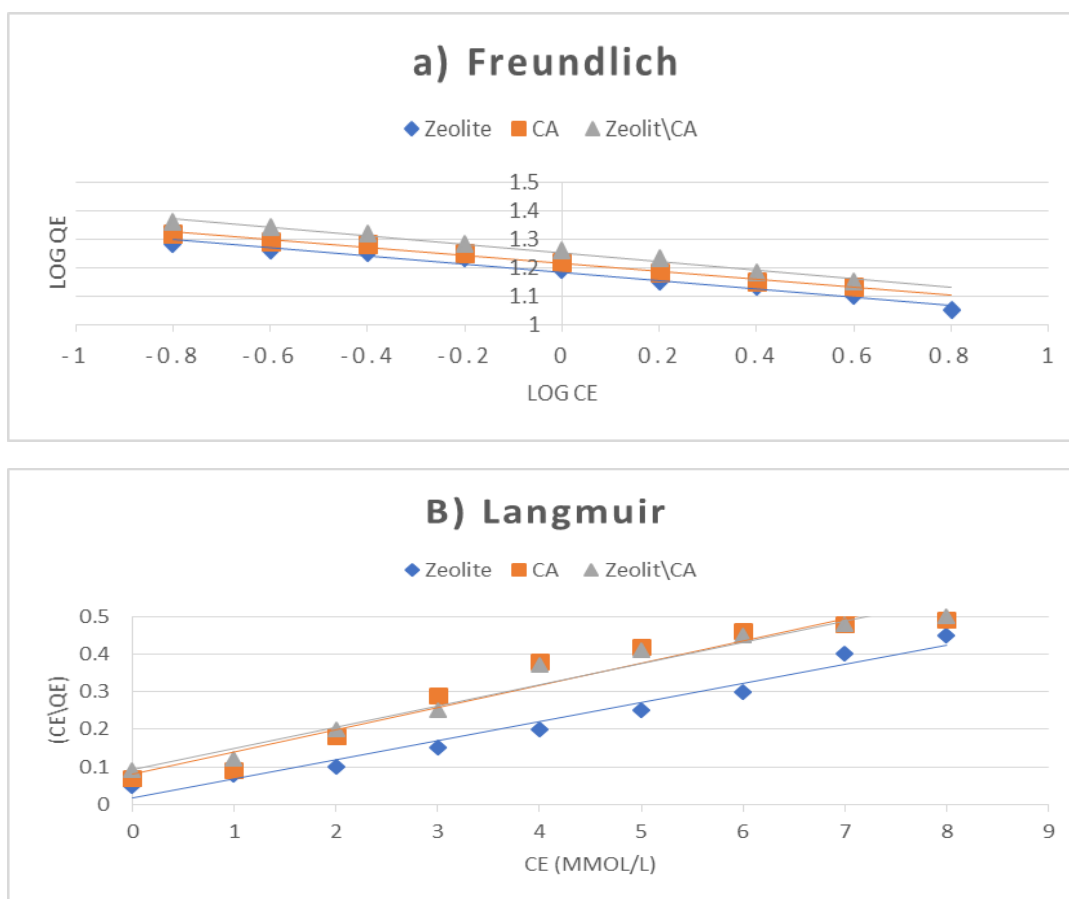


Figure17: Adsorption isotherm models: a) Freundlich, b) Langmuir models for ERY using three different adsorbents

10 mg/L of ERY adsorption onto ZCAB adsorbents were studied at room temperature (25 °C) for a period of time of 30 min using adsorbent dose of about 20 mg. The high regression coefficient (R^2) value can tell that this adsorption process is fitted better with Langmuir adsorption Isotherm (Table 4). So from this we can conclude that adsorption occurred mainly in a monolayer system and the surfaces of all ZCAB adsorbents are homogeneous.

Table 4: The parameters of Langmuir and Freundlich isotherms for the adsorption of ERY on ZCAB.

Isotherm Model				
Model	parameter	Zeolite	CA	Zeolite\CA
Langmuir	Slope	0.051	0.059	0.056
	$Y_{int.}$	0.035	0.023	0.037
	q_m	19.61	16.95	17.76
	K_L	560.22	743.38	477.47
	R^2	0.971	0.934	0.963
Freundlich	Slope	-0.0287	-0.0281	-0.0305
	$Y_{int.}$	1.33	1.35	1.40
	$K_f(mg^{(1-1/n)}g^{-1} L^{1/n})$	21.16	22.59	25.24
	N	-34.84	-35.59	-32.79
	R^2	0.975	0.988	0.985

4.4 Adsorption kinetic models

The experimental kinetic data for ERY adsorptions on predicted adsorbents were plotted following pseudo-1st-order and 2nd-order kinetic models and also as IPD model. The R^2 can tell how this process is suitable and follow that type of kinetic and its mechanism. The correlation coefficients and also

kinetics parameters can be found from the linear relation for each type that mentioned previously as shown in the (figure 18).

As seen in Fig. 18, pseudo-2nd modeling fit better for adsorption calculations relative to pseudo-1st modeling for three adsorbents.

However, the results obtained in pseudo-first-order modeling were still adequate to define the sorption kinetics of ERY, showing that the surface showed both chemi-sorption and physi-sorption adsorption processes. The regression coefficient (R^2) of all adsorbents in the pseudo second order are very close to 1 more than the one for pseudo first order. Also, the q_e calculated for the three adsorbents in the pseudo second order is very close to the experimental one as shown in (Table 5). It has been shown that the pseudo-second-order modeling showed an acceptable match to the adsorption compared to the pseudo-first-order modeling. The movement of ERY from aqueous solution to the adsorbents surfaces might be in different steps i.e., intra particle diffusion, film diffusion or both and that is the rate determining step. The intra particle diffusion model is shown in the next equation.

$$q_t = K_{pi}t^{1/2} + Ci$$

Where, Ci represents boundary layer thickness and K_{pi} is a constant. A plot between q_t vs. $t^{1/2}$ showed straight line with good value of correlation coefficient (R^2) leading to the applicability of intra particle diffusion model on all three forms of experimental data. For data that match the intra-particle

diffusion model, one sees two distinct areas, meaning that two stages are involved in the diffusion process: the external transfer of mass or boundary diffusion of the layer and the intra-particle or micropore diffusion. A greater slope of the first step than the second step suggests a faster adsorption operation, which is due to the more accessible adsorption sites at the initial stage [96].

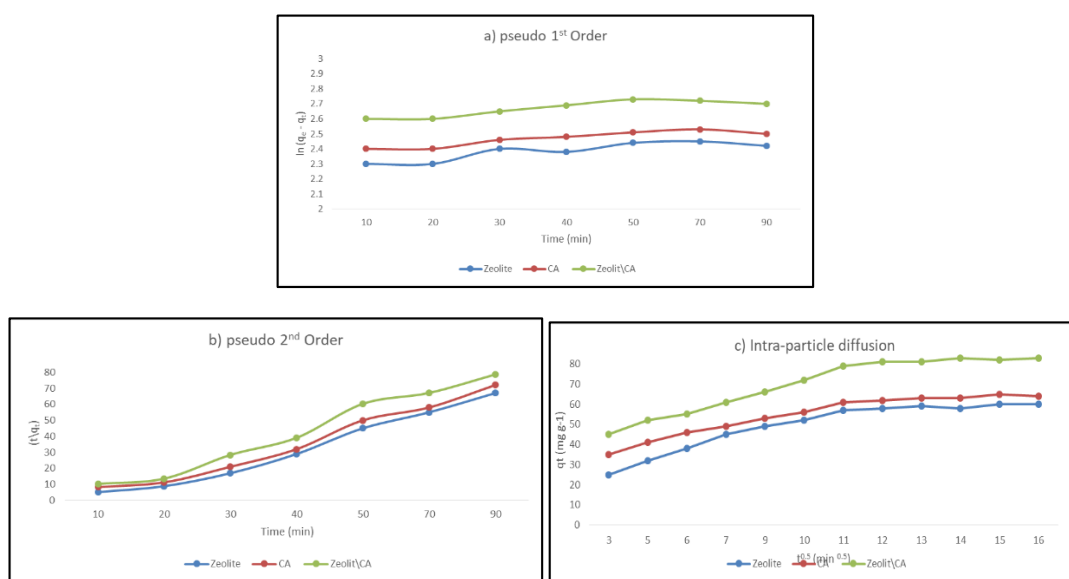


Figure 18: Kinetic models of for the adsorption of ERY by the three adsorbents at different time periods a) pseudo first order, b) pseudo second order, c) intraparticle diffusion.

Table 5: the parameters of pseudo-1st-order, pseudo-2nd-order for the adsorption of ERY onto ZCAB.

		Kinetic Model		
Parameter		Zeolite	CA	Zeolite\CA
1st Order	$q_{exp.}$	14.16	18.21	19.37
	$q_{calc.}$	13.92	17.21	18.23
	K_1	0.416	0.023	0.098
	R^2	0.962	0.973	0.988
2nd Order	$q_{calc.}$	10.62	8.17	9.23
	K_2	0.85	0.027	0.0335
	R^2	0.951	0.932	0.945

The experimental values of q_e are closer to calculated one in the pseudo-1st-order adsorption model, that's sign this adsorption follow the 1st-order model mechanism.

4.5 Adsorption thermodynamic

Van't Hoff equation was used to study adsorption thermodynamic; the thermodynamic parameters (ΔH , ΔS , and ΔG) for the adsorption of ERY onto ZCAB can be calculated from the slope and y-intercept of the graph of $\ln K$ versus $(1/T)$. Table 6 represents the values of the thermodynamic parameters (ΔH , ΔS , and ΔG) for the adsorption of ERY using ZCAB.

Table 6: the thermodynamic parameters for the adsorption of ERY on ZCAB

Thermodynamic				
Parameter	Temperature	Zeolite	CA	Zeolite\CA
ΔS (J mol ⁻¹)	20	0.08	0.06	0.03
ΔH (kJ mol ⁻¹)	20	-6200	-8500	-9600
ΔG (kJ mol ⁻¹)	20	-0.25	-0.35	-0.62
	25	-1.13	-1.17	-1.36
	30	-1.32	-1.56	-1.9
	35	-2.13	-2.78	-3.26
	45	-2.5	-3.5	-4.1

As shown in this table, the adsorption of ERY on ZCAB either in presence or absence of dissolved organic matter is exothermic process ($\Delta H < 0$) giving high % of removal as temperature increased, and also spontaneous ($\Delta G < 0$); furthermore, the all three processes go toward more disorder since the entropy parameter has positive values ($\Delta S > 0$).

4.6 Quantum Chemical Studies

The optimized geometry and calculated physical and quantum chemical quantities of ERY were given in Fig.19 and Table 7, respectively. Accordingly, the dipole moment (D), polarizability, (α), and first-order-hyper polarizability (β) values of ERY compound were determined as 4.421 D, 416.124 au, and 169.795 au, respectively. Also, the thermodynamic quantities ΔE , ΔH , and ΔG including the thermal correction were calculated at -2467.184 au, -2467.129 au, and -2467.269 au, respectively. As known well, the vibrational freedom constitutes a remarkable part of the thermal energy as well as the entropy (S) and heat capacity (C_v) for the molecular systems [102-104]. From Table 7, the thermal energy (ΔE) and vibrational movement contribution to the ΔE (ΔE_{vib}) were predicted at 730.238 kcal/mol and 728.461 kcal/mol, respectively. In addition, the C_v and S values of ERY compound were estimated at 207.438 cal/mol.K and 294.519 cal/mol.K, respectively, whereas the vibrational part of these quantities were determined at 201.476 cal/mol.K and 209.940 cal/mol.K, remarkably.

In addition, the QCPs are used successfully to assess the reactivity and its selectivity from the simple molecular systems [105, 106] to complex systems [107, 108]. In this work, the chemical reactivity tendency of ERY were assessed in light of the calculated QCPs and given in Table 7. The ΔE_{gap} and μ (eV) were determined at 9.757 eV and -4.506 eV, respectively. As known well, the hardness value is very helpful parameter to assess the chemical reactivity, especially in the evaluation of the adsorption processes. Hence, it

has been the main subject of a series theoretical investigations [109, 110] to be able to calculate it by using the different atomic and/or molecular constants and/or quantities such as ionization energies and electro negativities of the atoms in a specific molecule [111], atomic charges [112]. In addition, the molecular hardness has been reported to be able to use in the theoretical prediction of the lattice energies of the ionic crystals [113, 114]. In this work, the η and $\Delta\varepsilon_{\text{back-donat}}$ values of ERY were calculated at 4.879 eV and -1.220 eV, respectively. Furthermore, Table 7 displayed that the electro-donating power (0.182 au) of the ERY compound was calculated greater than the electro-accepting power (0.016 au), which affirmed that the ERY compound prefer the charge transfer to the metal surfaces. In past, corrosion inhibition efficiency was reported to increase with an increase of the electron-donating ability in case $\Delta N < 3.6$, and vice versa for $\Delta N > 3.6$ [115]. According to the ΔN ($0.032 < 3.6$) and electro-donating power values, the adsorption of the ERY towards the studied adsorbents is easily noticed to actualized via the charge transfer from the ERY compound to studied adsorbents.

Moreover, the possible nucleophilic (HOMO) and electrophilic (LUMO) attack sites of ERY compound were given in Fig. 20. The HOMO density was mostly amplified over the dimethyl amin ($-\text{N}(\text{CH}_3)_2$) functional and partially be scattered on the oxacyclohexane ring. On the other side, the LUMO broaden on the surrounding of $-(\text{C}=\text{O})-$ functional group of ERY. In addition, the MEP graphs displayed the electron- rich by red color ($V < 0$)

and poor by the blue color ($V > 0$) fields of the ERY compound. As expected, the $-C=O$ groups were covered by red color to electrophilic attacks and the H Atom of $-O-H$ group was marked by the blue color for the nucleophilic attacks. Also, the saturated C- chain of the ERY presented neutral attitude for both nucleophiles and electrophiles because of covered by the green color.

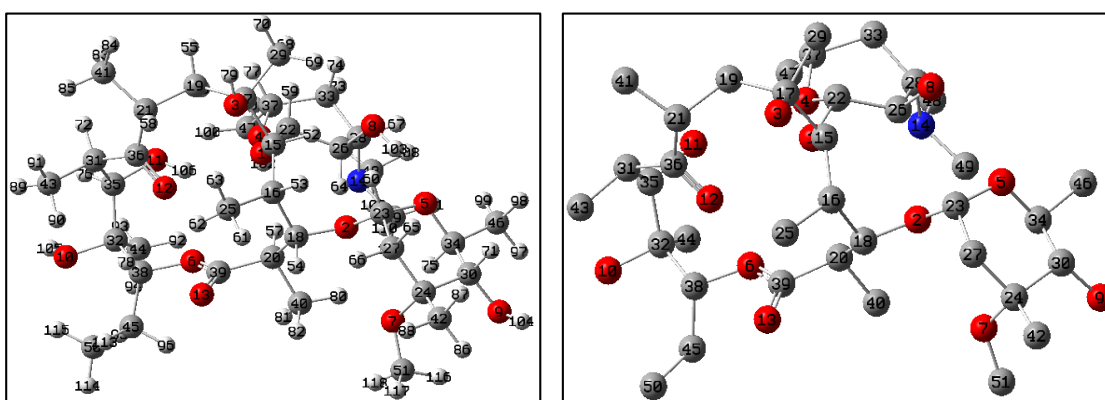


Figure 19: The optimized structures of ERY at HF/6-311G** level (left site with Hs and right side without Hs)

Table 7: The calculated physical and quantum chemical quantities of ERY at HF/6-311G** level

QCP		Physical Parameters	
HOMO (-I) (eV)	-9.385	DM (debye)	4.421
LUMO (-A) (eV)	0.372	α (au)	416.124
ΔE_{gap} (L-H) (eV)	9.757	β (au)	169.795
μ (eV)	-4.506	ΔE (au)	-2467.184
η (eV)	4.879	ΔH (au)	-2467.129
ω (eV)	2.081	ΔG (au)	-2467.269
ω^+ (au)	0.016	$\Delta E_{\text{thermal}}$ (kcal/mol)	730.238
ω^- (au)	0.182	$\Delta E_{\text{vib. (thermal)}}$ (kcal/mol)	728.461
ΔN (eV)	0.032	C_v (cal/molK)	207.438
$\Delta \epsilon_{\text{back-donat.}}$ (eV)	-1.220	$C_{\text{vib.}}$ (cal/molK)	201.476
ΔN_{max} (eV)	0.924	S (cal/molK)	294.519
		$S_{\text{vib.}}$ (cal/molK)	209.940

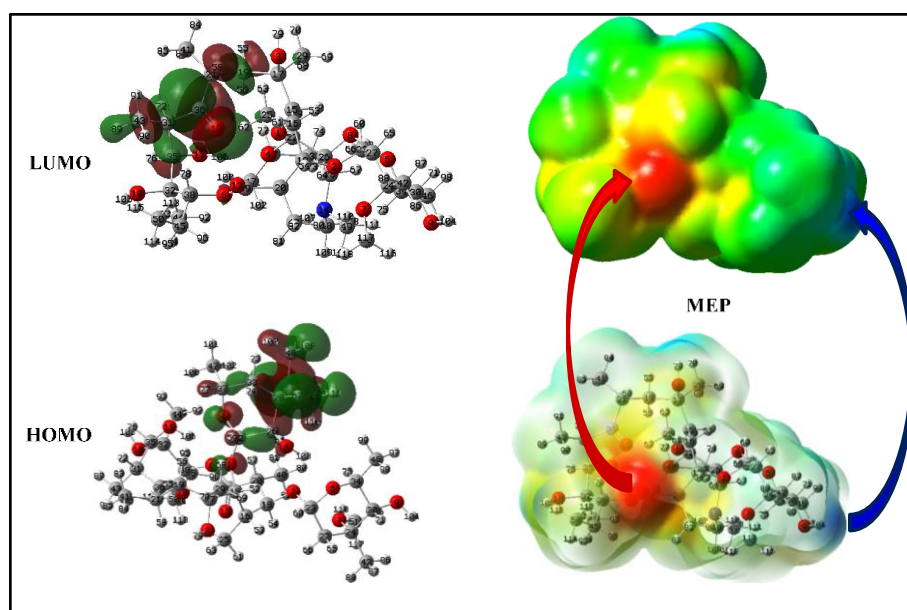


Figure 20: HOMO and LUMO (isoval:0.02), and MEP (isoval:0.0004) pilots of ERY at HF/6-311G level**

The chemical reactivity of many kind of molecular system [106, 116-118] have been also clarified by using the results of the second-order perturbative energy analysis. Table 8 summarized the lowering of the stabilization energy, possible interaction types, and the occupancies of both donor and acceptor orbitals. As expected the mainly saturated structure of ERY compound, the dominant interactions contributed to $E^{(2)}$ (62.33 kcal/mol) were sourced from the charge transfer to anti bonding orbital Π^* O13-C39 ($ED_j=0.15098e$) from non-bonding orbital LP (2) O6 ($ED_i=1.84800e$). Also, the hyper conjugations due to the charge movement from each filled orbital σ C31-C43 and σ C31-H72 to unfilled orbital Π^* C12-O36 were calculated with the $E^{(2)}$ of 4.77 kcal/mol and 2.39 kcal/mol, respectively, even if they did not contributed much to the $E^{(2)}$. From Table 2, the remaining interactions were due to the anomeric interactions and highest-energy interactions among them was predicted as the interaction LP (2) O13 ($ED_i=1.88472e$) \rightarrow σ^* O6-

C39 ($ED_j = 0.07615e$) in 42.55 kcal/mol. Similarly, the charge movement from the lone pair of the oxygen atom known as the strong electron-donating of -C=O group to neighbor orbitals had also great responsibility of the energy-lowering. Namely, the LP (2) O12 \rightarrow σ^* C21-C36 ($E^{(2)} = 24.58$ kcal/mol), LP (2) O12 \rightarrow σ^* C31-C36 ($E^{(2)} = 24.89$ kcal/mol), and LP (2) O13 \rightarrow σ^* C20-C39 ($E^{(2)} = 24.31$ kcal/mol) interactions had been also significant role in the lowering of the stabilization energy. As known well, that the -NH₂ group has also capability of the electron donating strongly. From Table 2, the charge movement from the N atom of the -NH₂ group to each of σ^* C28-H67, σ^* C48-H108, and σ^* C49-H111 interactions were calculated with the energy of 10.72, 10.83, and 10.74 kcal/mol, respectively. Here, it can be considered that these interactions have significant responsibility of the possible inter-molecular interactions due to the charge movement existed in a molecular system affecting of the polarity distribution on the surface.

Table 8: NBO Results for ERY at HF/6-311G level**

Donor(i)	ED _i /e	Acceptor (j)	ED _j /e	E ⁽²⁾ / kcal/mol	E(j)- E(i)/ a.u	F(i,j)/ a.u
σC31-C43	1.97272	Π*C12-O36	0.04962	4.77	1.06	0.064
σC31-H72	1.96974		2.39	0.92	0.042	
LP (2) O1	1.94227	σ* C15-H17	0.04194	9.47	1.08	0.091
		σ* C22-C26	0.04338	9.64	1.11	0.093
LP (2) O2	1.94036	σ* C18-H54	0.02444	8.56	1.18	0.090
		σ* C23-C27	0.03360	9.06	1.10	0.090
		σ* C23-H60	0.03251	9.90	1.15	0.096
LP (2) O3	1.96470	σ*C17-C19	0.03290	10.64	1.12	0.097
LP (2) O4	1.93923	σ* C22-C26	0.04338	9.30	1.11	0.091
		σ* C37-H77	0.02955	11.13	1.15	0.102
LP (2) O5	1.93444	σ* O2-C23	0.04266	15.27	1.12	0.117
LP (2) O6	1.84800	σ* C38-C45	0.02263	6.57	1.12	0.079
		Π* O13-C39	0.15098	62.33	0.74	0.192
LP (2) O7	1.94152	σ* C24-C30	0.04813	10.84	1.10	0.098
		σ* C51-H117	0.01658	9.50	1.12	0.093
LP (2) O8	1.96521	σ* C26-C28	0.03160	9.21	1.11	0.090
LP (2) O9	1.96742	σ* C24-C30	0.04813	9.41	1.13	0.092
LP (2) O10	1.96687	σ* C32-C35	0.04718	8.51	1.10	0.087
LP (2) O11	1.96259	σ* C31-C35	0.03166	9.18	1.10	0.090
LP (2) O12	1.91457	σ* C21-C36	0.05236	24.58	1.10	0.148
		σ* C31-C36	0.05427	24.89	1.11	0.149
LP (2) O13	1.88472	σ* O6-C39	0.07615	42.55	1.13	0.197
		σ* C20-C39	0.05115	24.31	1.08	0.147
LP (1) N14	1.90376	σ* C28-H67	0.02912	10.72	1.11	0.099
		σ* C48-H108	0.02251	10.83	1.07	0.098
		σ* C49-H111	0.02255	10.74	1.07	0.097

4.7 Desorption study

The stability and reusability of the three adsorbents is especially critical for widespread applications. The stability of the adsorbents was further studied by the adsorption-desorption recycling test as shown in Fig. 21. After each

run, the adsorbents washed twice with ethanol and then reused for the next step of adsorption [32, 119]. The results indicates that there is no substantial loss of adsorption site after three runs, indicating the higher reliability of the three adsorbents.



Figure21: Three cycles for each adsorbent showing excellent reuse.

4.8 Conclusion

Zeolite/cellulose acetate (ZCA) in blend fiber for adsorption of erythromycin residue showed a very good result, furthermore, a functionalized Zeolite/cellulose acetate (ZCA) in blend fiber have a higher adsorption capacity and the percent of removal at the optimum conditions increased, and showed a very good thermal and chemical stabilities, and hence it can be used as perfect adsorbent to uptake erythromycin residue from wastewater. The results showed that all adsorption followed Langmuir

adsorption isotherm. The mechanism of all reactions followed pseudo^{1st} order kinetic adsorption model. With respect to thermodynamic, the parameters proved that all processes are exothermic ($\Delta H < 0$), spontaneous ($\Delta G < 0$), and processes go toward disorder state ($\Delta S > 0$). The QCPs revealed that the adsorption of the ERY towards the studied adsorbents actualize via the charge transfer from the ERY compound to studied adsorbents, because of the ΔN ($0.032 < 3.6$) and electro-donating power values. The MEP plots pointed out that the $-C=O$ groups were covered by red color to electrophilic attacks and the H Atom of $-O-H$ group was marked by the blue color for the nucleophilic attacks. The NBO analysis of the ERY indicated that the anomeric and hyper-conjugative interactions have chiefly responsibility of the possible inter-molecular interactions because of the charge movement affecting of the polarity distribution on the surface.

The regeneration of adsorbent did not highly reduce the removal efficiency, and the regenerated adsorbents showed a good percentage removal after 3rd use for the removal of erythromycin residue, so it can be used multiples. A sample was collected from a real mixture of wastewater and treated with the ZCAB. The removal efficiency of ERY present in the wastewater sample was high and remarkable.

4.8 Recommendations

1. This work aims to remove one of the widespread by erythromycin antibiotics adsorption process onto ZCAB materials.

2. Know how much the source of water in Palestine polluted with erythromycin antibiotics.
3. Furthermore, it should be economically feasible to use such materials in water treatment process, and to devote an extra effort in the development of the Zeolite/cellulose acetate (ZCA) in blend fiber material industry.
4. Try to engineer specialized and commercially available filters using those materials.
5. To use other adsorption materials or other efficient technique for the removal of erythromycin antibiotics.
6. The widely use of pharmaceutical products in various areas has led to the worldwide pollution in the environment and water in Palestine polluted. However, effective purification of water pollution by erythromycin antibiotics remains a great challenge must to increase the level of awareness of people about how to properly use antibiotics and not to overuse them.

References

1. Chon, K., et al., *Fouling characteristics of dissolved organic matter in fresh water and seawater compartments of reverse electrodialysis under natural water conditions*. Desalination, 2020. **496**: p. 114478.
2. El-Zawily, A.E.-S., et al., *Application of magnetic field improves growth, yield and fruit quality of tomato irrigated alternatively by fresh and agricultural drainage water*. Ecotoxicology and environmental safety, 2019. **181**: p. 248-254.
3. Kizskiel-Taudul, I., *Determination of antihistaminic pharmaceuticals in surface water samples by SPE-LC-MS/MS method*. Microchemical Journal, 2021. **162**: p. 105874.
4. Arshad, M.S., et al., *Coronavirus disease (COVID-19) and immunity booster green foods: A mini review*. Food Science & Nutrition, 2020. **8**(8): p. 3971-3976.
5. Bungau, S., et al., *Aspects of excessive antibiotic consumption and environmental influences correlated with the occurrence of resistance to antimicrobial agents*. Current Opinion in Environmental Science & Health, 2020.
6. Bhowmick, S., et al., *Algal metabolites: An inevitable substitute for antibiotics*. Biotechnology Advances, 2020: p. 107571.

7. Barchiesi, M., et al., *Presence and fate of microplastics in the water sources: focus on the role of wastewater and drinking water treatment plants*. Journal of Water Process Engineering, 2020: p. 101787.
8. Stevens, J.L. and K.C. Jones, *Quantification of PCDD/F concentrations in animal manure and comparison of the effects of the application of cattle manure and sewage sludge to agricultural land on human exposure to PCDD/Fs*. Chemosphere, 2003. **50**(9): p. 1183-1191.
9. Farré, M., *Remote and in-situ devices for the assessment of marine contaminants of emerging concern and plastic debris detection*. Current Opinion in Environmental Science & Health, 2020.
10. Mery-Araya, C., et al., *Using carbon substrate as a selection pressure to enhance the potential of aerobic granular sludge microbial communities for removing contaminants of emerging concern*. Bioresource technology, 2019. **290**: p. 121705.
11. Bui, D.N. and T.T. Minh, *Investigation of TNT red wastewater treatment technology using the combination of advanced oxidation processes*. Science of The Total Environment, 2021. **756**: p. 143852.
12. Ma, H., et al., *Liberation and recovery of Cr from real tannery sludge by ultrasound-assisted supercritical water oxidation treatment*. Journal of Cleaner Production, 2020. **267**: p. 122064.

13. Yu, H., et al., *Improved Norfloxacin degradation by urea precipitation Ti/SnO₂-Sb anode under photo-electro catalysis and kinetics investigation by BP-neural-network-physical modeling*. Journal of Cleaner Production, 2021. **280**: p. 124412.
14. Tabassum, S., *A combined treatment method of novel Mass Bio System and ion exchange for the removal of ammonia nitrogen from micro-polluted water bodies*. Chemical Engineering Journal, 2019. **378**: p. 122217.
15. Oturan, N., et al., *Electrocatalytic destruction of the antibiotic tetracycline in aqueous medium by electrochemical advanced oxidation processes: effect of electrode materials*. Applied Catalysis B: Environmental, 2013. **140**: p. 92-97.
16. Ou, H., et al., *Selective removal of erythromycin by magnetic imprinted polymers synthesized from chitosan-stabilized Pickering emulsion*. Journal of hazardous materials, 2015. **289**: p. 28-37.
17. Khan, M.H., H. Bae, and J.-Y. Jung, *Tetracycline degradation by ozonation in the aqueous phase: proposed degradation intermediates and pathway*. Journal of hazardous materials, 2010. **181**(1-3): p. 659-665.
18. Jorfi, M. and E.J. Foster, *Recent advances in nanocellulose for biomedical applications*. Journal of Applied Polymer Science, 2015. **132**(14).

19. Abitbol, T., et al., *Nanocellulose, a tiny fiber with huge applications*. *Current opinion in biotechnology*, 2016. **39**: p. 76-88.
20. Schilling, K.E., *Investigating local variation in groundwater recharge along a topographic gradient, Walnut Creek, Iowa, USA*. *Hydrogeology journal*, 2009. **17**(2): p. 397-407.
21. Cosgrove, W.J. and F.R. Rijsberman, *World water vision: making water everybody's business*. 2014: Routledge.
22. Abdelmadjid, B. and S. Omar, *Assessment of groundwater pollution by nitrates using intrinsic vulnerability methods: A case study of the Nil valley groundwater (Jijel, North-East Algeria)*. *African Journal of Environmental Science and Technology*, 2013. **7**(10): p. 949-960.
23. Edition, T., *Guidelines for Drinking-water Quality*. *WHO Chronicle*, 2008. **1**(3): p. 334-415.
24. Pal, P., *Treatment and disposal of pharmaceutical wastewater: toward the sustainable strategy*. *Separation & Purification Reviews*, 2018. **47**(3): p. 179-198.
25. Guo, Y., P. Qi, and Y. Liu. *A review on advanced treatment of pharmaceutical wastewater*. in *IOP Conference Series: Earth and Environmental Science*. 2017. IOP Publishing.
26. Szabó, L., et al., *Electron beam treatment for tackling the escalating problems of antibiotic resistance: eliminating the antimicrobial activity*

- of wastewater matrices originating from erythromycin*. Chemical Engineering Journal, 2017. **321**: p. 314-324.
27. Hua, T., et al., *Degradation performance and microbial community analysis of microbial electrolysis cells for erythromycin wastewater treatment*. Biochemical Engineering Journal, 2019. **146**: p. 1-9.
28. Michael-Kordatou, I., et al., *Erythromycin oxidation and ERY-resistant Escherichia coli inactivation in urban wastewater by sulfate radical-based oxidation process under UV-C irradiation*. Water research, 2015. **85**: p. 346-358.
29. Shekhawat, S., N. Kulshreshtha, and A. Gupta, *Tertiary treatment technologies for removal of antibiotics and antibiotic resistance genes from wastewater*, in *Removal of Toxic Pollutants Through Microbiological and Tertiary Treatment*. 2020, Elsevier. p. 1-41.
30. Chen, N., et al., *Analysis of the effect of erythromycin wastewater degradation by Fenton method*. Asian Journal of Chemistry, 2013. **25**(13): p. 7208-7210.
31. Amin, M.M., et al., *Influence of the antibiotic erythromycin on anaerobic treatment of a pharmaceutical wastewater*. Environmental science & technology, 2006. **40**(12): p. 3971-3977.
32. Gholamiyan, S., M. Hamzehloo, and A. Farrokhnia, *RSM optimized adsorptive removal of erythromycin using magnetic activated carbon:*

- Adsorption isotherm, kinetic modeling and thermodynamic studies.* Sustainable Chemistry and Pharmacy, 2020. **17**: p. 100309.
33. Louvet, J.-N., et al., *Adverse effects of erythromycin on the structure and chemistry of activated sludge.* Environmental Pollution, 2010. **158**(3): p. 688-693.
34. Qu, X., P.J. Alvarez, and Q. Li, *Applications of nanotechnology in water and wastewater treatment.* Water Res, 2013. **47**(12): p. 3931-46.
35. Afzal, A., et al., *Physico-Chemical Processes.* Water Environment Research, 2011. **83**(10): p. 994-1091.
36. Pérez, J.A.S., et al. *A two-stage scheme for pesticide degradation Integration of photocatalysis and biological oxidation.* in *13th International Biotechnology Symposium and Exhibition (第 13 届 IUPAC 国际生物工程会议)*. 2008. 大连理工大学.
37. Martín, M.B., et al., *Degradation of a four-pesticide mixture by combined photo-Fenton and biological oxidation.* Water Research, 2009. **43**(3): p. 653-660.
38. Kannan, N. and M.M. Sundaram, *Kinetics and mechanism of removal of methylene blue by adsorption on various carbons—a comparative study.* Dyes and pigments, 2001. **51**(1): p. 25-40.
39. Naushad, M., Z. Al-Othman, and M. Islam, *Adsorption of cadmium ion using a new composite cation-exchanger polyaniline Sn (IV) silicate:*

- kinetics, thermodynamic and isotherm studies*. International Journal of Environmental Science and Technology, 2013. **10**(3): p. 567-578.
40. Akhtar, M., et al., *Low cost sorbents for the removal of methyl parathion pesticide from aqueous solutions*. Chemosphere, 2007. **66**(10): p. 1829-1838.
 41. Ali, I., *New generation adsorbents for water treatment*. Chemical reviews, 2012. **112**(10): p. 5073-5091.
 42. Ioannidou, O.A., et al., *Preparation of activated carbons from agricultural residues for pesticide adsorption*. Chemosphere, 2010. **80**(11): p. 1328-1336.
 43. Gonzalez-Pradas, E., et al., *Adsorption of malathion from aqueous solution on homoionic bentonite samples*. Agrochimica, 1993. **37**(1-2): p. 104-110.
 44. Rauf, N., et al., *Equilibrium, thermodynamics and kinetics studies for the removal of alpha and beta endosulfan by adsorption onto bentonite clay*. Chemical engineering journal, 2012. **192**: p. 369-376.
 45. Naushad, M., Z. ALOthman, and M. Khan, *Removal of malathion from aqueous solution using De-Acidite FF-IP resin and determination by UPLC–MS/MS: Equilibrium, kinetics and thermodynamics studies*. Talanta, 2013. **115**: p. 15-23.

46. Bolto, B., et al., *Removal of THM precursors by coagulation or ion exchange*. Water research, 2002. **36**(20): p. 5066-5073.
47. Humbert, H., et al., *Natural organic matter (NOM) and pesticides removal using a combination of ion exchange resin and powdered activated carbon (PAC)*. Water Research, 2008. **42**(6-7): p. 1635-1643.
48. Camel, V., *Solid phase extraction of trace elements*. Spectrochimica acta. Part B, Atomic spectroscopy, 2003. **58**(7): p. 1177-1233.
49. Poole, C.F., *New trends in solid-phase extraction*. TrAC Trends in Analytical Chemistry, 2003. **22**(6): p. 362-373.
50. Vismara, E., et al., *Alpha cellulose from industrial and agricultural renewable sources like short flax fibres, ears of corn and wheat-straw and its transformation into cellulose acetates*. Journal of Materials Chemistry, 2009. **19**(45): p. 8678-8686.
51. Puls, J., S.A. Wilson, and D. Hölder, *Degradation of cellulose acetate-based materials: a review*. Journal of Polymers and the Environment, 2011. **19**(1): p. 152-165.
52. Biswas, A., et al., *Process for obtaining cellulose acetate from agricultural by-products*. Carbohydrate polymers, 2006. **64**(1): p. 134-137.

53. Rahman, M., N. Hasnida, and W.W. Nik, *Preparation of zeolite Y using local raw material rice husk as a silica source*. Journal of Scientific Research, 2009. **1**(2): p. 285-291.
54. Baghdad, K. and A.M. Hasnaoui, *Zeolite–cellulose composite membranes: Synthesis and applications in metals and bacteria removal*. Journal of Environmental Chemical Engineering, 2020. **8**(4): p. 104047.
55. Gazicki, M., W. James, and H. Yasuda, *Colloids and surfaces a: physicochemical and engineering aspects*. Journal of Polymer Science: Letters Polymer Edition, 1985. **23**: p. 639-645.
56. Widiastuti, N., et al., *Cellulose Acetate/Zeolite-A Membrane for Ni²⁺ Adsorption*. CHEMICAL ENGINEERING, 2019. **72**.
57. Zhong, Z., et al., *Oriented two-dimensional zeolitic imidazolate framework-L membranes and their gas permeation properties*. Journal of Materials Chemistry A, 2015. **3**(30): p. 15715-15722.
58. Song, Z., et al., *Molecular sieving film prepared by vacuum filtration for the efficient removal of tetracycline antibiotics from pharmaceutical wastewater*. Advances in Materials Science and Engineering, 2019. **2019**.
59. Song, Z., et al., *Removal of tetracycline residue from pharmaceutical wastewater by using 3D composite film*. Chemical Engineering Journal, 2018. **348**: p. 898-907.

60. Low, Z.-X., et al., *Effect of addition of two-dimensional ZIF-L nanoflakes on the properties of polyethersulfone ultrafiltration membrane*. Journal of membrane science, 2014. **460**: p. 9-17.
61. Grassi, M., et al., *Removal of emerging contaminants from water and wastewater by adsorption process*, in *Emerging compounds removal from wastewater*. 2012, Springer. p. 15-37.
62. Dada, A., et al., *Langmuir, Freundlich, Temkin and Dubinin–Radushkevich isotherms studies of equilibrium sorption of Zn²⁺ unto phosphoric acid modified rice husk*. IOSR Journal of Applied Chemistry, 2012. **3**(1): p. 38-45.
63. Balarak, D., et al., *Langmuir, Freundlich, Temkin and Dubinin–radushkevich isotherms studies of equilibrium sorption of ampicillin unto montmorillonite nanoparticles*. Journal of Pharmaceutical Research International, 2017: p. 1-9.
64. Sharma, R. and P. Saini, *Graphene-based composites and hybrids for water purification applications*, in *Diamond and Carbon Composites and Nanocomposites*. 2016, IntechOpen.
65. Zhou, L., et al., *Kinetics and thermodynamics studies of pentachlorophenol adsorption on covalently functionalized Fe₃O₄@SiO₂–MWCNTs core–shell magnetic microspheres*. Chemical Engineering Journal, 2014. **257**: p. 10-19.

66. Desta, M.B., *Batch sorption experiments: Langmuir and Freundlich isotherm studies for the adsorption of textile metal ions onto teff straw (Eragrostis tef) agricultural waste*. Journal of thermodynamics, 2013. **2013**.
67. Tran, H.N., et al., *Mistakes and inconsistencies regarding adsorption of contaminants from aqueous solutions: a critical review*. Water research, 2017. **120**: p. 88-116.
68. Toulmin III, P. and P.B. Barton Jr, *A thermodynamic study of pyrite and pyrrhotite*. Geochimica et Cosmochimica Acta, 1964. **28**(5): p. 641-671.
69. Panlener, R., R. Blumenthal, and J. Garnier, *A thermodynamic study of nonstoichiometric cerium dioxide*. Journal of Physics and Chemistry of Solids, 1975. **36**(11): p. 1213-1222.
70. Štejfa, V., et al., *Thermodynamic study of selected monoterpenes*. The Journal of Chemical Thermodynamics, 2013. **60**: p. 117-125.
71. Massa, F., A. Coppola, and F. Scala, *A thermodynamic study of sorption-enhanced CO₂ methanation at low pressure*. Journal of CO₂ Utilization, 2020. **35**: p. 176-184.
72. Rodchanasuripron, W., M. Seadan, and S. Suttiruengwong, *Properties of non-woven polylactic acid fibers prepared by the rotational jet spinning method*. Materials Today Sustainability, 2020. **10**: p. 100046.

73. Bagaev, A., T. Bukanova, and I. Chubarenko, *Spring cold water intrusions as the beginning of the cold intermediate layer formation in the Baltic sea*. Estuarine, Coastal and Shelf Science, 2021. **250**: p. 107141.
74. Wang, Z., et al., *Microfiltration performance of electrospun nanofiber membranes with varied fiber diameters and different membrane porosities and thicknesses*. Polymer, 2017. **114**: p. 64-72.
75. Zhang, Q., X. Lu, and L. Zhao, *Preparation of polyvinylidene fluoride (PVDF) hollow fiber hemodialysis membranes*. Membranes, 2014. **4**(1): p. 81-95.
76. Güler, E., et al., *Performance-determining membrane properties in reverse electrodialysis*. Journal of membrane science, 2013. **446**: p. 266-276.
77. Gaussian09, R.A., *1, mj frisch, gw trucks, hb schlegel, ge scuseria, ma robb, jr cheeseman, g. Scalmani, v. Barone, b. Mennucci, ga petersson et al., gaussian*. Inc., Wallingford CT, 2009. **121**: p. 150-166.
78. Roothaan, C.C.J., *New developments in molecular orbital theory*. Reviews of modern physics, 1951. **23**(2): p. 69.
79. Pople, J. and R.K. Nesbet, *Self-consistent orbitals for radicals*. The Journal of Chemical Physics, 1954. **22**(3): p. 571-572.

80. Krishnan, R., et al., *Self-consistent molecular orbital methods. XX. A basis set for correlated wave functions*. The Journal of chemical physics, 1980. **72**(1): p. 650-654.
81. McLean, A. and G. Chandler, *Contracted Gaussian basis sets for molecular calculations. I. Second row atoms, Z= 11–18*. The Journal of chemical physics, 1980. **72**(10): p. 5639-5648.
82. Koopmans, T., *Über die Zuordnung von Wellenfunktionen und Eigenwerten zu den einzelnen Elektronen eines Atoms*. Physica, 1934. **1**(1-6): p. 104-113.
83. Parr, R.G., L.v. Szentpály, and S. Liu, *Electrophilicity index*. Journal of the American Chemical Society, 1999. **121**(9): p. 1922-1924.
84. Parr, R.G. and R.G. Pearson, *Absolute hardness: companion parameter to absolute electronegativity*. Journal of the American chemical society, 1983. **105**(26): p. 7512-7516.
85. Pearson, R.G., *Absolute electronegativity and hardness correlated with molecular orbital theory*. Proceedings of the National Academy of Sciences, 1986. **83**(22): p. 8440-8441.
86. Pearson, R.G., *Absolute electronegativity and hardness: application to inorganic chemistry*. Inorganic chemistry, 1988. **27**(4): p. 734-740.

87. Gazquez, J.L., A. Cedillo, and A. Vela, *Electrodonating and electroaccepting powers*. The Journal of Physical Chemistry A, 2007. **111**(10): p. 1966-1970.
88. Gómez, B., et al., *Quantum chemical study of the inhibitive properties of 2-pyridyl-azoles*. The Journal of Physical Chemistry B, 2006. **110**(18): p. 8928-8934.
89. Foster, a.J. and F. Weinhold, *Natural hybrid orbitals*. Journal of the American Chemical Society, 1980. **102**(24): p. 7211-7218.
90. Reed, A.E. and F. Weinhold, *Natural localized molecular orbitals*. The Journal of chemical physics, 1985. **83**(4): p. 1736-1740.
91. Reed, A.E., L.A. Curtiss, and F. Weinhold, *Intermolecular interactions from a natural bond orbital, donor-acceptor viewpoint*. Chemical Reviews, 1988. **88**(6): p. 899-926.
92. Brunauer, S., P.H. Emmett, and E. Teller, *Adsorption of gases in multimolecular layers*. Journal of the American chemical society, 1938. **60**(2): p. 309-319.
93. Barrett, E.P., L.G. Joyner, and P.P. Halenda, *The determination of pore volume and area distributions in porous substances. I. Computations from nitrogen isotherms*. Journal of the American Chemical society, 1951. **73**(1): p. 373-380.

94. Fan, G., et al., *Isolation of cellulose from rice straw and its conversion into cellulose acetate catalyzed by phosphotungstic acid*. Carbohydrate polymers, 2013. **94**(1): p. 71-76.
95. Armaroli, T., et al., *Effects of crystal size and Si/Al ratio on the surface properties of H-ZSM-5 zeolites*. Applied Catalysis A: General, 2006. **306**: p. 78-84.
96. Hong, S.H., Y. Cho, and S.W. Kang, *Highly porous and thermally stable cellulose acetate to utilize hydrated glycerin*. Journal of Industrial and Engineering Chemistry, 2020. **91**: p. 79-84.
97. Mostafapour, F.K., M. Dashtizade, and D. Balarak, *Adsorption thermodynamics, kinetics and mechanism for the adsorption of erythromycin onto multi-walled carbon nanotubes*. Journal of Pharmaceutical Research International, 2018: p. 1-11.
98. Fateme, B., et al., *Synthesis of porous graphene nanocomposite and its excellent adsorption behavior for Erythromycin antibiotic*. Наносистемы: физика, химия, математика, 2020. **11**(2).
99. Danalıoğlu, S.T., et al., *Efficient removal of antibiotics by a novel magnetic adsorbent: Magnetic activated carbon/chitosan (MACC) nanocomposite*. Journal of Molecular Liquids, 2017. **240**: p. 589-596.

100. Ribeiro, M.H. and I.A. Ribeiro, *Modelling the adsorption kinetics of erythromycin onto neutral and anionic resins*. Bioprocess and biosystems engineering, 2003. **26**(1): p. 49-55.
101. Hanbali, G., et al., *Enhanced ibuprofen adsorption and desorption on synthesized functionalized magnetic multiwall carbon nanotubes from aqueous solution*. Materials, 2020. **13**(15): p. 3329.
102. Sandler, S.I., *An introduction to applied statistical thermodynamics*. 2010: John Wiley & Sons.
103. McQuarrie, D.A., *Statistical thermodynamics*. 1973.
104. Herzberg, G., *Molecular Spectra and molecular structure-Vol I*. Vol. 1. 2013: Read Books Ltd.
105. Serdaroğlu, G. and J. Ortiz, *Ab initio calculations on some antiepileptic drugs such as phenytoin, phenbarbital, ethosuximide and carbamazepine*. Structural Chemistry, 2017. **28**(4): p. 957-964.
106. Serdaroğlu, G., S. Kaya, and R. Tourir, *Eco-friendly sodium gluconate and trisodium citrate inhibitors for low carbon steel in simulated cooling water system: Theoretical study and molecular dynamic simulations*. Journal of Molecular Liquids, 2020. **319**: p. 114108.
107. Junejo, R., et al., *Experimental and DFT Modeling Studies for the Adsorptive Removal of Reactive Dyes from Wastewater*. Separation Science and Technology, 2021: p. 1-15.

108. Al-Otaibi, J.S., et al., *Adsorption of Adipic acid in Al/BN/P nanocages: DFT investigations*. Journal of Molecular Modeling, 2021. **27**(4): p. 1-7.
109. Parr, R.G. and J.L. Gazquez, *Hardness functional*. The Journal of Physical Chemistry, 1993. **97**(16): p. 3939-3940.
110. Chaudhary, S., et al., *Theoretical computation of normalised radii, density and global hardness as a function of orbital exponent*. Journal of Mathematical Chemistry, 2021. **59**(4): p. 1014-1028.
111. Kaya, S. and C. Kaya, *A new method for calculation of molecular hardness: a theoretical study*. Computational and Theoretical Chemistry, 2015. **1060**: p. 66-70.
112. Kaya, S. and C. Kaya, *A new equation for calculation of chemical hardness of groups and molecules*. Molecular Physics, 2015. **113**(11): p. 1311-1319.
113. Kaya, S. and C. Kaya, *A simple method for the calculation of lattice energies of inorganic ionic crystals based on the chemical hardness*. Inorganic chemistry, 2015. **54**(17): p. 8207-8213.
114. Islam, N. and S. Kaya, *Conceptual density functional theory and its application in the chemical domain*. 2018: CRC Press.

115. Lukovits, I., E. Kalman, and F. Zucchi, *Corrosion inhibitors—correlation between electronic structure and efficiency*. *Corrosion*, 2001. **57**(1): p. 3-8.
116. Jacob, J.M., et al., *Mixed ligand copper (II) chelates derived from an O, N, S-donor tridentate thiosemicarbazone: Synthesis, spectral aspects, FMO, and NBO analysis*. *Polyhedron*, 2020. **189**: p. 114736.
117. Serdaroglu, G., *Harmine derivatives: a comprehensive quantum chemical investigation of the structural, electronic (FMO, NBO, and MEP), and spectroscopic (FT-IR and UV-Vis) properties*. *Research on Chemical Intermediates*, 2020. **46**(1): p. 961-982.
118. Mustafa, E. and G. Serdaroglu, *A Computational Study of 1-substituted methyl 9-methyl-9H-pyrido [3, 4-b] indole-3-carboxylate: Quantum Chemical Descriptors, FMO and NBO Analysis*. *Cumhuriyet Science Journal*, 2017. **38**(4): p. 138-155.
119. Jodeh, S., et al., *Magnetic nanocellulose from olive industry solid waste for the effective removal of methylene blue from wastewater*. *Environmental Science and Pollution Research*, 2018. **25**(22): p. 22060-22074.

جامعة النجاح الوطنية

كلية الدراسات العليا

استخدام الزيوليت / خلاات السليلوز (ZCA) في مزيج
الألياف لإزالة الأريثروميسين من محلول مائي دراسة
تجريبية ونظرية

إعداد

إسراء فيصل أحمد عرمان

بإشراف

أ. د. شحدة جودة

أ. د. عثمان حامد

قدمت هذه الأطروحة استكمالاً لمتطلبات الحصول على درجة الماجستير في الكيمياء في كلية الدراسات العليا، جامعة النجاح الوطنية، نابلس فلسطين

2021

ب

استخدام الزيوليت / خلاات السليلوز (ZCA) في مزيج الألياف لإزالة الأريثروميسين من محلول

مائي دراسة تجريبية ونظرية

إعداد

إسراء فيصل احمد عمران

بإشراف

أ. د. شحدة جودة

أ. د. عثمان حامد

الملخص

نعلم ان كثرة استخدام المنتجات الصيدلانية وخاصة المضادات الحيوية في مختلف المجالات ادى الى تلويث المياه والبيئة وهدفنا هو تحسين وتطوير طريقة لتنقية مياه الصرف الصحي من المضاد الحيوي الأريثروميسين بواسطة غشاء من خلاات السليلوز والزيوليت كمادة ماصة حيث تم تحديد عدد المواقع القابلة للتبديل في الهياكل الممتازة والأريثروميسين ومن خلال عملنا اظهرت النمذجة الزائفة من الدرجة الاولى ملاءمة افضل لامتصاص الأريثروميسين من النمذجة الدرجة الثانية مما يدل على ان سطح المواد الممتازة عرض جميع عمليات الامتصاص الفيزيائية والكيميائية بواسطة كلا المادتين الماصتين ايضا تمت مناقشة نموذج متساوي الحرارة لانجمير وفرندلخ؛ لايجاد ان افضل درجة حرارة للامتصاص تم ملاحظتها بشكل افضل بمتساوي الحرارة لانجمير وكما ان دراسة الديناميكا الحرارية للامتصاص.

تمثل قيم المعلمات الديناميكية الحرارية ΔH و S و G ، وامتصاص الأريثروميسين على خيوط الزيوليت وخلاات السليلوز إما في وجود أو عدم وجود مادة عضوية مذابة هو عملية طاردة للحرارة ($\Delta H < 0$) مما يعطي نسبة عالية منا لإزالة مع ارتفاع درجة الحرارة، وكذلك بشكل تلقائي ($\Delta G < 0$)؛ علاوة على ذلك، تتجه جميع العمليات الثلاث نحو المزيد من الفوضى نظرًا لأن مع قيم الانتروبي موجبة؛ كما لا يظهر تحليل الامتصاص اي خسارة كبيرة في مواقع الامتزاز بعد ثلاث دورات مما يشير الى الاستقرار والمرونة من المواد الماصة الثلاث مما يشير الى قابيلة تكرار قوية لاستخدامها المحتمل في عمليات الامتزاز دون تلويث البيئة.